

Optimization of case studies in HSS bolted connections.

Alberto Soliveres Lledó

Thesis submitted for the degree of
Master of Science in Materials
Engineering,
Industrial Engineering studies

Thesis supervisors:

Prof. dr. ir. Dimitri Debruyne
Ing. Carlos Jiménez

Assessor:

Prof. Eva María Sánchez Orgaz

© Copyright KU Leuven

Without written permission of the thesis supervisors and the author it is forbidden to reproduce or adapt in any form or by any means any part of this publication. Requests for obtaining the right to reproduce or utilize parts of this publication should be addressed to Faculteit Ingenieurswetenschappen, Kasteelpark Arenberg 1 bus 2200, B-3001 Heverlee, +32-16-321350.

A written permission of the thesis supervisors is also required to use the methods, products, schematics and programmes described in this work for industrial or commercial use, and for submitting this publication in scientific contests.

Preface

I would like to express my gratitude to the university researcher team for helping me to feel welcomed in the university since the first moment. To my tutor for giving me the necessary help and guidance throughout the project process and to my family and friends for proving to be a great support when it is most needed. My most sincere gratitude goes to all of them.

Alberto Soliveres Lledó

Contents

Preface	i
Abstract	iv
List of Figures and Tables	v
List of Abbreviations and Symbols	vii
1 Introduction	1
1.1 Heavy duty machines and profitability	1
1.2 Introduction to HSS	2
1.3 Introduction to the DAF case	3
1.4 Subject of study	4
2 Material selection and joining methods	5
2.1 Steel alloys	5
2.2 Joining methods	9
2.3 Conclusion	12
3 Specimens design and manufacture	13
3.1 Test specimens design	13
3.2 Specimen manufacture	16
3.3 Assembly	21
3.4 Conclusion	22
4 Failure modes	25
4.1 Multiaxial fatigue criteria	25
4.2 Criteria application	26
4.3 Conclusion	26
5 Analysis and evaluation of the results	27
5.1 General meshing parameters	27
5.2 Mesh convergence	29
5.3 Numerical calculations	30
5.4 Conclusion	34
6 Testing procedure	37
6.1 Test set-up	37
6.2 Correlation with the numerical model (DIC)	38
6.3 Results and discussions	39

6.4 Conclusion	42
7 Conclusion and future work lines	45
Appendices	49
A Drawing compilation	51
B Design parametrization and scripting	63
B.1 Design parametrization	63
B.2 Abaqus scripting	64
Bibliography	67

Abstract

The aim of the project is the definition, analytical study and test validation of a complex load bolted connection in HSS.

Steel is a widely used and developed alloy due to its high tensile strength and low cost, properties which, makes it a perfect material for multiple purposes: from machine construction, auto mobiles and tools to be a crucial part in buildings and infrastructures.

Despite all the improvements made in the steel alloys the mechanical failure of the components is still happening this days, and in some cases this failure is accompanied with human and economical losses. That is why the study of steel mechanical failure is so important. To prevent the material failure a deep understanding of the machine operation modes is needed, that is why the evaluation of steel behaviour of the components and its operation modes is so important.

The objective is to determine a joint that allows a failure mode originated by a complex loads set. This is why a design capable of being tested under the combined action of bending efforts and shear stress conditions is built.

This union, subjected to a complex state of loads is motivated by the determination of which is the crucial failure mode in the elements subjected to several loading conditions. A union is presented in which the influence of the bending stresses and surface fretting conditions can be modified by a parameter variation as it is the joining angle between the models.

The increase or decrease of this joining angle is set to show different load conditions in the contact interface. This approach means to represent a design precedent and to establish design lines in the bolted connection construction under a load combination.

To perform this investigation a parametric study of different joint set-up under this load combined conditions is carried out with the aim of evaluating this fracture mechanism. In this study the finite element approach is used in order to analyse a variety of test specimens.

Finally a good correspondence is found between the analytical model, the test results and the DIC which which endorses the model definition and allows it to be used for the validation of other case studies.

List of Figures and Tables

List of Figures

1.1	Heavy duty vehicles	1
1.2	CAT truck and excavator	2
1.3	Load modes of bolted connections	4
2.1	Banana plot from World Auto Steel	6
2.2	Steel alloys comparison	7
2.3	Estimation of the thickness reduction that can be achieved by switching from grade 1 to grade 2 steel based on Eq. (2.1)	8
2.4	Principal Joining methods	10
2.5	Welding methods	11
2.6	General welding terminology	11
3.1	Test proposals	14
3.2	Final test design 45° assembly set-up	15
3.3	Original S700 MC sheet	16
3.4	Cutting processes comparison	17
3.5	Pieces cut with water jet machine	18
3.6	Bending parameters definition	19
3.7	Bending process	20
3.8	Plates produced	21
3.9	Sandblasting process	22
5.1	FEM of the plate assembly	28
5.2	Finite element models for a bolted joint	29
5.3	Normalized maximum principal stress stress distribution along the normalized centreline of the specimen for different mesh sizes	30
5.4	Calculation time and element number of the overall assembly for each mesh size in the contact zone	31
5.5	Normalized maximum principal stress distribution along the normalized centreline of the specimen for the different bend angles	32
5.6	Normalized shear stress distribution along the normalized centreline of the specimen for the different bend angles	33

5.7	Normalized contact slip along the normalized centreline of the specimen for the different bend angles	34
5.8	Contact pressure and contact status contour plots for the 60° plate configuration	34
5.9	Rad agreement tension transition	35
5.10	Fatemi-SWT correlation for the 45° plate assembly	35
5.11	Fatigue criteria application for each case	36
6.1	DIC correlation process	39
6.2	Dynamical stiffness behaviour in the tests	40
6.3	Specimen results for the fixed axial of 6kN load test	40
6.4	Specimen results for same maximal principal stress magnitude in the fracture area	41
6.5	Numerical model correlation with the test	41
6.6	Fatigue crack transversal surface identification	42
6.7	S-N distribution and theoretical curves for the tested specimens	43
7.1	V. Venugopa equivalent shell model bolted connection approaches	46
7.2	V. Venugopal multi-bolt plate analysis with equivalent shell model	46
7.3	Introduction of a sharper angle value in the plate parameters	47
B.1	NX expressions module	64
B.2	Angle parameter modifications	65
B.3	Model representations	66
B.4	Abaqus python Scripting integration flow diagram	66

List of Tables

2.1	Mild Steel alloys - Mechanical properties	6
2.2	HSS alloys - Mechanical properties	7
2.3	S700MC chemical composition	9
3.1	Garnet 80 mesh chemical composition	17
3.2	Process details for a group of plates of $\angle 45^\circ, \angle 60^\circ$ and $\angle 75^\circ$	18
6.1	Test approaches	37
6.2	DIC parameters	38

List of Abbreviations and Symbols

Abbreviations

HSS	High-Strength Steel
HAZ	Heat Affected Zone
WM	Welding Material
HSLA	High-Strength Low-Alloy
UHSS	Ultra-High-Strength Steel
UTS	Ultimate Tensile Strength
HCF	High Cycle Fatigue
LCF	Low Cycle Fatigue
SLBJ	Single lap bolted joint
DLBJ	Double lap bolted joint
SWT	Smith-Watson-Topper
FS	Fatemi-Socie
FEA	Finite Element Analysis
FEM	Finite Element Modelling
DIC	Digital Image correlation

Symbols

E	Young's modulus
σ_y	Yield strength
t_1	Grade 1 steel plate thickness
t_2	Grade 2 steel plate thickness
Re_1	Grade 1 steel Yield strength
Re_2	Grade 2 steel Yield strength
T_r	Thickness reduction percentage
T	Torque
K_{nut}	Nut factor
$F_{preload}$	Preload force
R	Original bending radius
r	Final bending radius
t	Plate thickness
f	Frequency
$(\sigma_{n,max})$	Maximum normal stress
(ε_1)	Maximal strain range
$(\sigma_{n,max})$	Maximum normal stress
R_s	Load ratio

Chapter 1

Introduction

1.1 Heavy duty machines and profitability

Trucks, harvesters, and heavy duty equipment [Fig. 1.1](#) and [1.2](#) are machines that are developed in a highly competitive market, defined by a constant search for increase profitability. This harsh environment forces the manufacturers to be in constant research and development in order to provide machines that could carry more load or show further improvements over their competitors, in general lines, making them more lucrative.



(a) DAF truck



(b) CNH Harvester

Figure 1.1: Heavy duty vehicles

The problem is found when we realize that in order to provide them with an enhanced weight carrying or resistance capabilities bigger steel frames are needed or a thickness increment on them is inevitable. This contributions to the structure are translated in weight increments in the vehicle frames that have to be taken in account due to the the weight limitations imposed by the government or the European Union in this case [\[17\]](#) to this vehicles.

This limitations are forcing that any improvements in the structures have to be checked thoroughly to ensure compliance with the regulations. Since the limits are becoming narrower the difficulties in making some progress in the load carrying capacity are intensified due to the weight gain that this entails in the structure. Further modifications in the construction of this equipment have to be made in order

to obtain an overall weight reduction.

Thus a weight reduction in this machines is crucial in order to continue rising the weight that this machines can carry and evolve in this competitive market.



Figure 1.2: CAT truck and excavator

To do so the overall trend is the substitution of the traditional structural steel alloys for HSS ones which are able to maintain the strength of the structure while reducing the profile section and hence the weight of the overall structure.

Due to these machine operation modes the frame of these equipments is subject to high peak and cyclic loads which lead to a fatigue damage in the brittle HSS welds, limiting by far the potential that HSS can introduce, this is when the search for other types of joints within the framework of trucks comes into play, among which the bolted joints stand out since this joining method does not show a material structure modification as the ones produced by the welding like HAZ.

1.2 Introduction to HSS

The total or partial replacement of structural steel components to HSS ones in the frame construction of this machines carries several advantages:

1. Lighter structure
2. Increased payload
3. Reduced self weight loads
4. Reduced fuel consumption

These qualities play a crucial role in developing equipment that is able to carry a greater load while ensuring that the vehicles will be within the maximum weights set by the institutions.

1.2.1 HSS frames connections

Traditionally the heavy duty machine frames were assembled by joining its longitudinal and cross members using welding methods. This technique is proven to provide a fair union and a correct stress transmission between the members built in mild steel alloys.

But when the HSS is introduced the welded joints shows unsatisfactory fatigue resistant and lead to a brittle fracture in the members in the HAZ, which limits the enhanced properties of the HSS largely. To prevent this condition post weld treatments have been introduced and proved to help increasing the fatigue resistance of the welded joints under fatigue cyclic loading, as it is shown by S. Vanrostenberghe et al. [63] but with the drawback of its high cost that makes the overall process unprofitable in some cases

This is the motivation that has lead to a research through the joining methods to be used in order to have acceptable fatigue resistance while keeping the cost in a reasonable value. Among other options the bolted joint comes in as a possible replacement, substituting the welded connections by bolted one as the main joining method between HSS parts

The material properties of HSS as well as the joining methods between them are developed in more depth in [chapter 2](#).

1.3 Introduction to the DAF case

As it is mentioned in the previous chapter an investigation is being carried out to verify the capacity of the joints between HSS by means of screw connections. Companies like DAF and CNH are developing new durability processes to evaluate the fatigue resistance of bolted connections in its frames.

In the DAF case a research is being carried out in order to develop guidelines for optimal design of bolt connections as well as simulation techniques for reliable fatigue prediction of bolt connections. Those are compiled under the DuraMech-project.

In order to develop this tests the loads in the frame bolted connections have been identified and defined for the testing procedures. In plane loads, out of plane bending and the combination of both are the most common load cases in the bolted connections in a truck or a heavy duty machine. This loads are originated mainly due to the deformation of the chassis caused by the road input and the internal resonance of the chassis itself

As we can see in figure [Fig. 1.3](#) the load modes are described as follow:

1. Out-of-plane loads (F_z , M_x , M_y). Bending of the connected plate around the bolt head.
2. In-plane loads (F_x , F_y , M_z). Apply an in plane force to the plate, resulting in a shear force to the bolted connection

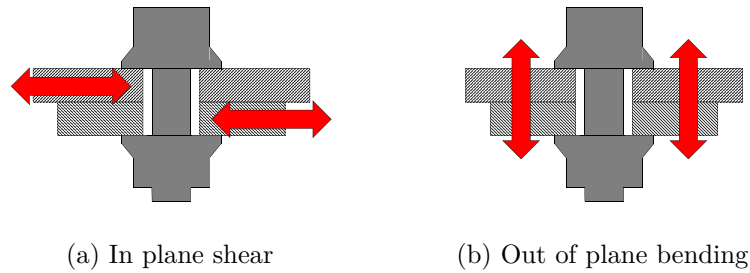


Figure 1.3: Load modes of bolted connections

This load modes are proposed to be evaluated in a complex joint connection, able to represent both load cases simultaneously. This entails the beginning of a new line of research in screwed joints, with the definition of a model able to represent a combined failure behaviour to determine which load condition is more determinant for the and how to design in consequence.

1.4 Subject of study

As it is introduced in the previous section a complex load state bolted connection is defined for this project. The bolted connection will be designed using HSS, steel grade which, the [chapter 2](#) introduces and compares among the mild steel alloys to determine the advantages the HSS has in relation to the structural steel alloys. The bolted joining method is also introduced in this chapter.

The specimen design parameters and considerations are determined in [chapter 3](#) where the manufacturing process steps are described as well. To determine the loading conditions, estimate the fatigue life and make any further analysis consideration a numerical model of the samples is built. This model is evaluated for the fatigue failure criteria described in [chapter 4](#) and its results are used as a baseline for the definition of the tests in [chapter 6](#).

The testing chapter is used to validate the numerical model with the DIC technique and a correlation with the tested samples. The failure modes of each sample are described an the fatigue curves for the specimen variations are determined.

Finally the overall results and statements are exposed in [chapter 7](#) which also includes the future lines of work that this research opens up.

Chapter 2

Material selection and joining methods

In this chapter a comparative is made among the mild steel alloys and the HSS ones, discussing the best joining methods for each case. The aim of this section is to expose the qualities of each steel group in order to justify the use of HSS alloys in heavy duty machines and equipment construction.

2.1 Steel alloys

It is included within the definition of steel the Fe-C alloys with a Carbon content under 2.11% of its weight. That is the point where the division between “Cast irons” and steel alloys is found.

Steels micro structured is based on the eutectoid portion of the FE-C diagram. This lower carbon weight percentage in the alloy allows the material to develop a much more ductile fracture behaviour instead of the brittle fracture observed in the cast iron.

At the present time the companies are researching for new materials for the construction of their equipment, with alternatives that bring better fatigue and static results or a weight decrease in the structure. A graph is published by World Auto Steel [55] in order to identify the future steel necessities in the automotive industry .This chart is depicted in Fig. 2.1. From from it can be observed how the steel grades a bundled by their stress-strain behaviour, but the important part of it is the definition of the the future development path towards the 3rd AHSS steel alloys, defined by high strength and a great ductility in the same material, properties which, enable the design of lighter weight vehicle structures.

This statements motivates the research of HSS to replace the mild alloys in machine construction. To endorse the World Auto Steel claims a comparison is made among the steel grades distinguishing two groups according to the molecular properties and the alloying elements that defines each steel group. The stress-strain behaviour of each group behaviour is also displayed.

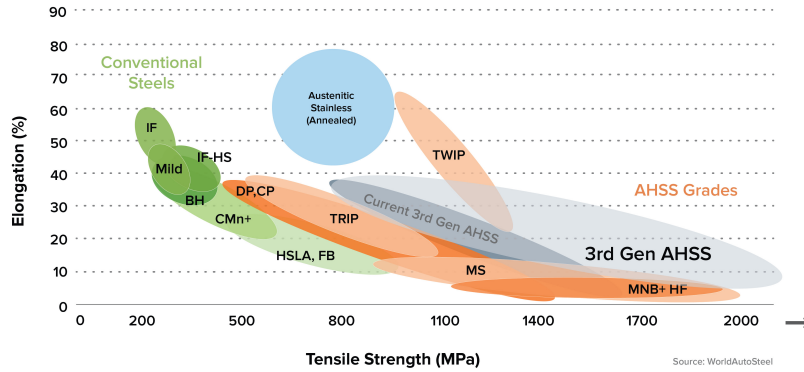


Figure 2.1: Banana plot from World Auto Steel [44]

Grade 1 steels

Mild structural steels are used in many ways and their application can be diverse. This grade group is particularly useful because offers a unique combination of good welding properties with guaranteed strengths. Structural steel is an extremely adaptable product and is often favoured by the engineer trying to maximise strength or fatigue behaviour of a structure while minimising its weight, compared with other construction materials.

The construction industry is one of the highest consumers of this structural steel, using it for all purpose but this steel type is also highly valued by machine builders.

This group is encompassed within the green area of the Fig. 2.1 under the conventional steel set, and clusters the S235,S275 and S355 alloys which data is stored in Table 2.1. This values are obtained from the European steel standards [2].

	Young modulus [GPa]	Yield stress [MPa]	UTS [MPa]	Elongation [%] ¹
S235	210	235	360	37
S275	210	275	410	28
S355	210	355	490	27

Table 2.1: Mild Steel alloys - Mechanical properties

HSS-HSLA

High strength and HSLA are micro alloyed steels that arose in response to the reduction requirement of the weight of the vehicles and the manufacturers pursuit for increasing the benefits. This alloys represent steels with very low carbon percentages (Typically below 0.2%), and about $\leq 1\%$ by weight such as Mn, P, Si, Cr, Ni, Mo.

¹Uniform strain up to

These steels are cold-formed formed by a controlled thermomechanically-process to obtain a very fine grain structure with high values of elastic limit and resistance, together with a low ductile-brittle transition temperature, as described in [54].

Extremely high strength is always associated with higher amounts of alloying elements and tends to result in higher hardenability which leads to a higher risk for brittle fracture and hydrogen induced cracking in welded constructions [67]. The compromise between the steel resistance and ductility behaviour needs to be reach.

It has been more than 3 decades since steel is available as an improved and reinforced steel alloy, overtaking the traditional steel alloys due to its increases in the yield strength while maintaining the density ratio.

The HSS stress-strain behaviour is compiled in Fig. 2.2 From it we can observe that values of up to 1060.5 MPa UTS can be reach with this alloys, meaning a extremely high load-bearing capacity behaviour. The HSS alloys mechanical properties are listed in Table 2.2.

	Young modulus [GPa]	Yield stress [MPa]	UTS [MPa]	Elongation [%] ²
S500MC	210	562.7	658	13.7
S700MC	210	731.1	801.7	11.8
S960MC	210	976.8	1060.5	3.2

Table 2.2: HSS alloys - Mechanical properties

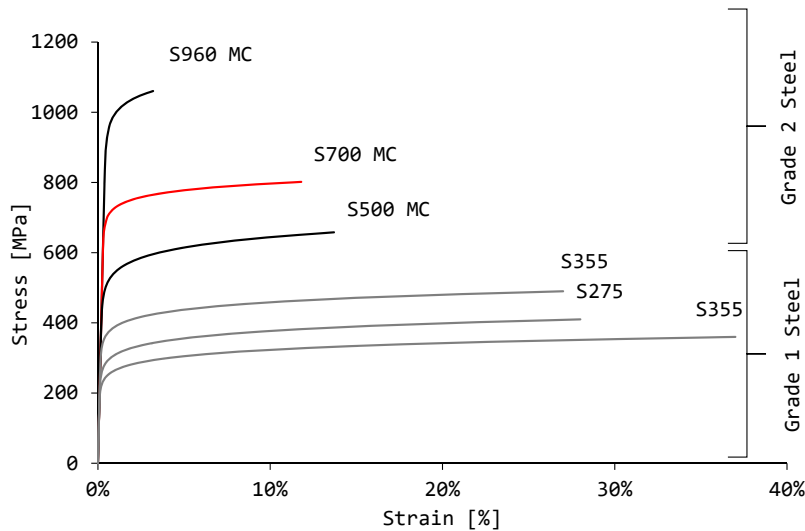


Figure 2.2: Steel alloys comparison

To compare both steel grades applications the steel manufacturer, Arcelor Mittal [41] proposes an equation that has been modified to Eq. (2.1). This expression

²Uniform strain up to

2. MATERIAL SELECTION AND JOINING METHODS

determines the thickness reduction percentage in the usage of HSS replacing mild steel alloys. A practical example for this equation application is used to show the high weight percentage reduction HSS demonstrates.

$$t_2 = t_1(Re_1/Re_2)^{1/2}; T_R(\%) = 1 - t_1/t_2 \quad (2.1)$$

In the Fig. 2.3 a bar diagram is displayed with the approximate thickness reduction when changing from Grade 1 to Grade 2 steel. This figure illustrates the weight reduction in the structure when HSS is applied in replacement of the traditional structural steel alloys as a thickness reduction in the frame's profiles.

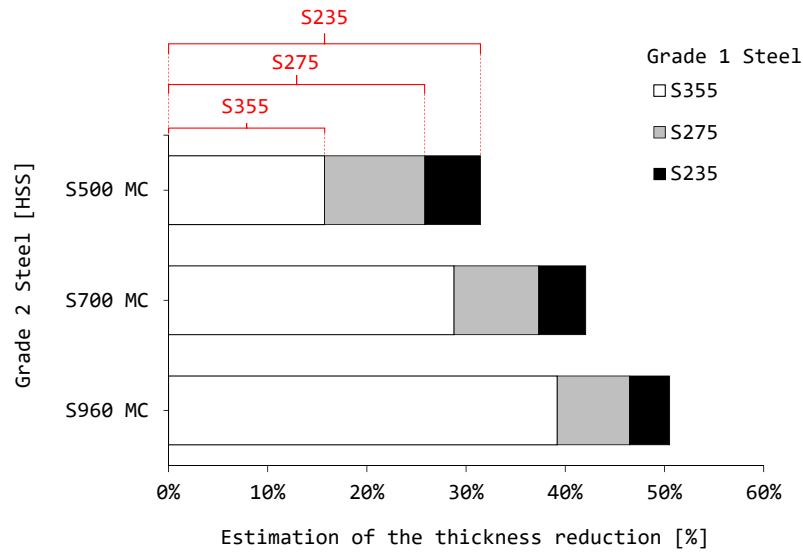


Figure 2.3: Estimation of the thickness reduction that can be achieved by switching from grade 1 to grade 2 steel based on Eq. (2.1)

For instance if a a Class 8 Truck tractor frame defined in [47] weights 2.040 lb (~ 926 kg). If the assumption that the frame is built using S355 mild steel is made and that this material is replaced with S700 HSS a maximum $\sim 28\%$ weight reduction can be theoretically achieved. A ~ 266 kg reduction in the structure weight is obtained with this relation which means a drastical weight reduction in the structure while maintaining the components resistance values intact (Note that these are only guidance values to show the capacity in weight reduction that the introduction of HSS entails, and do not represent any determining value.)

These statements are considered to be adequate to determine the HSS as a highly recommend material for machinery construction since the and is determined as the material grade for the project tests.

It must be taken into account when selecting the HSS construction material that the increase in the yield strength leads to a loss in the maximum elongation. That is why from the HSS steel alloys Table 2.2 the S700MC HSS is selected as the

model design material, due to the compromise between high strength and ductility that it presents and that make it an excellent candidate for the tests. The chemical properties for the S700MC are listed in [Table 2.3](#)

C (%)	Mn (%)	P (%)	S (%)	Si (%)	Al (%)	Nb (%)	Ti (%)	Mo (%)	B (%)	V (%)
≤ 0.12	≤ 2.1	≤ 0.025	≤ 0.015	≤ 0.6	≥ 0.015	≤ 0.09	≤ 0.22	≤ 0.5	≤ 0.005	≤ 0.2

Table 2.3: S700MC chemical composition ^{3,4}

This chemical composition is defined by the 10149-2 standard [[15](#)].

2.2 Joining methods

Due to the production processes, design specifications, process economy or any other needs, joints needs to be made between steel parts in order to conform the frames or structures in the machine building.

To perform this link between metal parts a wide range of connections are being used as depicted in [Fig. 2.4](#), and is the designer task to select the appropriate joining method for each situation attending to the joint parameters and specifications.

From this methods of joining, emphasis is placed on the frame connections used by trucks and heavy duty machines that are composed in their majority from welded and bolted joints owing to the high loads and vibrations that occur in these members and the resistance and of the joint has to be assured. Returning to the DAF case a deep development and comparative among those methods is exposed.

2.2.1 Welding

As it is described by M. Khan [[30](#)]: ” The welding is a process of joining two metals permanently using localised coalescence resulting from a combination of temperature, pressure and metallurgical conditions.”

The different types of welding based on the source of energy required to do the joining process by ISO 4063 [[25](#)] are compiled in [Fig. 2.5](#).

When two metals are welded a microstructure is formed in the HAZ and in the WM. This microstructures determine the mechanical properties of the joint. Pre-heating and post welding treatments are used to control the microstructures and the properties of welding by controlling the cooling rates. Studies have been carried out in order to improve the behaviour of the HAZ and the WM by controlling a set of parameters in the welded joints.

Z. Burzi et al [[29](#)] centres its study in the fatigue fracture of HSS steel alloys welded with MAW. It is observed that crack initiation and therefore the failure area starts in the HAZ coarse-grain region or in the transition and its developed through the HAZ for low and high cycle stress. This experiment sets demonstrate that the

⁴In percent by weight

⁴the sum of Nb, V and Ti < 0.220 is guaranteed according to EN 10149-2 [[15](#)]

⁵Hemming, Mechanical interlocking and many more

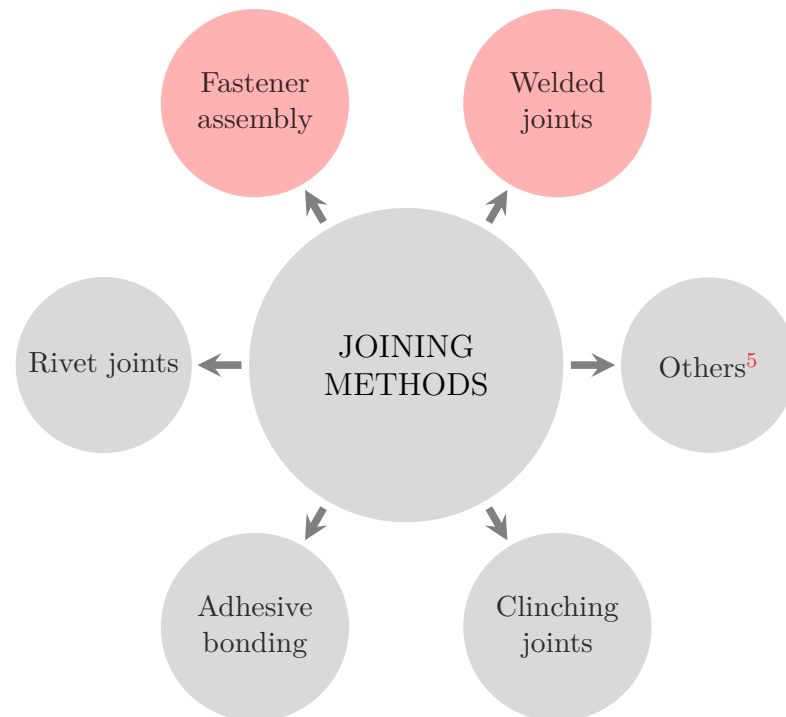


Figure 2.4: Principal Joining methods

fatigue resistance of both the WM and the HAZ are reduced compared to the parent metal and emphasizes that this has to be taken into account when designing welded joints in HSS.

From these investigations we can conclude that welded joints represent a durable union between steel plates but since the material properties in the joint are modified due to the applied heat in the material fractures can appear.

2.2.2 Hardware Assembly

The Screw joint / fastener assembly is the most commonly used semi permanent joint. In this type of joint bolt, nuts and washers are used to join the metal parts.

The bolted connection determined for this project is a through bolted connection that is used to join sheet metal specimens with a bolt and nut assembly.

To perform this connection type a hole with the correct clearance is made in the joint parts. The hardware assembly is then placed in it and fixed with the adequate tightening torque.

In a bolted connection design once the loads in the structure have been defined is the designer job to define the placement, size and number of bolts, but also the preload. The preload needs to be defined for each assembly and many factors needs to be considered in order to reach a proper clamping force. As it is recommended in [8] and [68] the preload for permanent fasteners needs to be at least the 90%

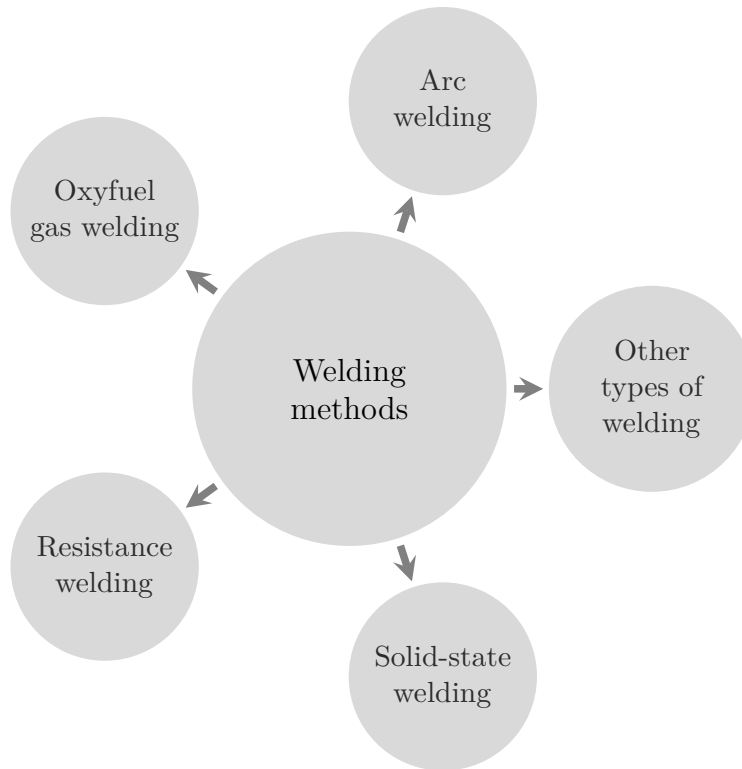
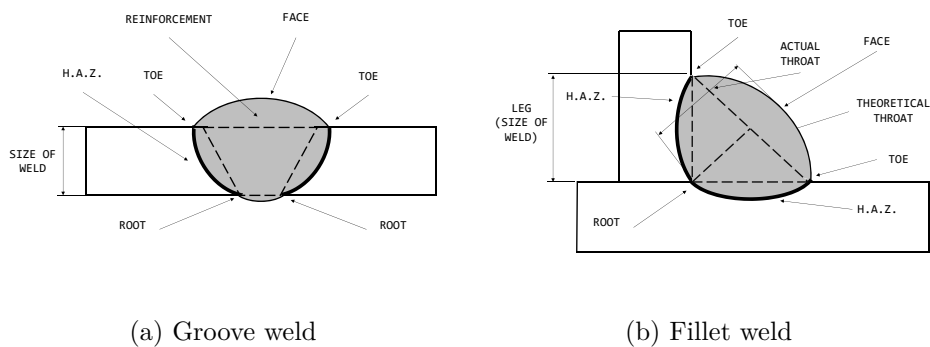


Figure 2.5: Welding methods



(a) Groove weld

(b) Fillet weld

Figure 2.6: General welding terminology

of the proof strength but this value can change depending on the manufacturer considerations and internal standards.

To perform a tightening analysis and definition the torque-tension equation defined in [52] is used Eq. (2.2). This equation defines a linear relationship between the torque and tension variables and is used to define the torque magnitude when the clamping force is defined in the union.

$$T = K_{nut} \cdot d_{bolt} \cdot F_{preload} \quad (2.2)$$

A special emphasis is placed on the tightening torque correct definition. Since the clamping force for joints under cyclic conditions, as the ones used in the project, is important to extend the fatigue life of the joint. As it is shown by A. Benhamena et al. [5].

2.3 Conclusion

From this chapter the selection of HSS is justified against the mild steel alloys as it provides an crucial weight reduction in the structure for the same resistance in the members involved. This statement is confirmed by the Fig. 2.3 where a minimum thickness reduction of 15% and values up to the 50% reduction in the member's thickness can be achieved with this steel grade replacement. Leading to a substantial weight reduction in the structures.

The joining methods are also discussed in this chapter. Welded connections are a durable and connection method widely used in the frames construction but the drawback of the possibility of a sudden failure in the HAZ due to a fatigue loads has us investigate other joining methods in which the materials retain their molecular properties. The bolted joints offer a high resistance union and are determined to be studied in the joint proposed in the project.

Chapter 3

Specimens design and manufacture

The aim of the project is the model design for a joint that is able to reproduce both load states depicted in [Fig. 1.3](#). This specimen is mean to be used in order to determine the influence of each load state in the failure mode. In order to accomplish this task a set of models needs to be defined with a parameter variation that can modify the plates load states and therefore the failure mode.

Hence in this chapter the design decisions for the model are explained and the manufacturing process is reported.

3.1 Test specimens design

The specimens are designed to represent the combined load condition mentioned in this chapter heading. From the research carried out by M. Mohammadpour et al. [\[42\]](#) and S. Heimbs et al. [\[21\]](#) it is determined that 90° plates connection (L-shaped plates defined as coach-peel bolted joints) subjected to axial fatigue loading have a failure mode is determined by the bending moment in the bolt flange. On the other hand bolted flat plates (SBLJ, DBLJ) in axial fatigue stress load condition present a fretting fatigue failure mode as it is shown by Hämäläinen et al. [\[20\]](#), C. Jiménez et al. [\[28\]](#) and H. Talemi et al. [\[22\]](#) in their respective studies. This specimen design is meant to be a complex connection able to reach a combination of both loads conditions, with the possibility of determining the influence of each one in the fracture mode with the angle determined between the joined plates.

With this in mind the model design proposal of plates joined by means of a screwed connection in a determined angle disposition is started. As a complex union is mean to be tested it is imposed as a starting criterion to make 4 screws bolted joint so that the effect of each bolt row and and its influence on the testing results can be evaluated. A representative set of the initial proposals is stored in [Fig. 3.1](#). These models are discussed with the research personnel to check the design specifications and to check whether the university equipment is capable of performing tests on them.

The test proposal 1 [Fig. 3.1a](#) to [Fig. 3.1c](#) represents the initial plate set-up for the bolted connection. This connection is distinguished by showing the shear component as the principal failure factor. This is due to its design resulting from including an angled joint in an SLBJ connection.

The test proposal 2 [Fig. 3.1d](#) to [Fig. 3.1f](#) in contrast to the first proposal is shown to have the bending moment as the determining failure factor since the design is inspired in the L-plate bolted connection with an angular variation.

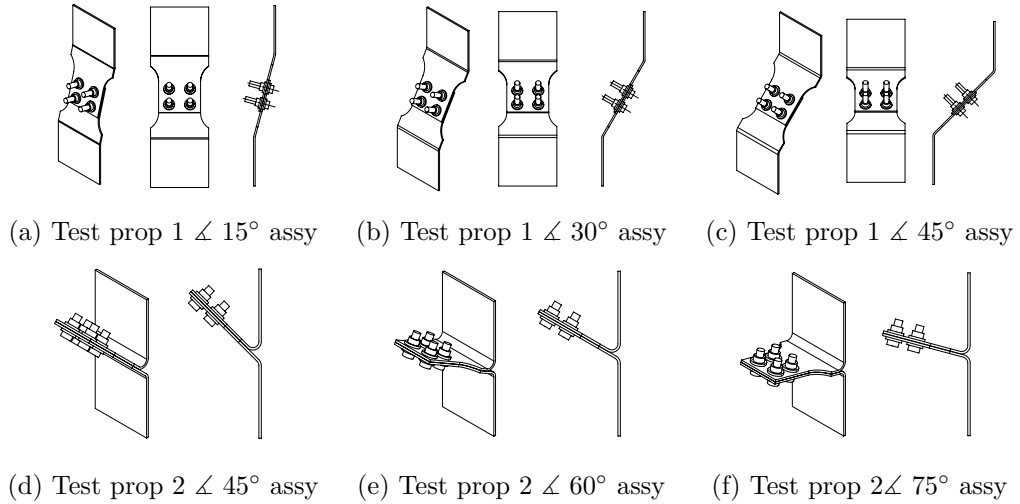


Figure 3.1: Test proposals

Those two testing models approaches are evaluated and it is found that the testing machine available in the faculty does not accept the plate's longitudinal plane misalignment determined by angular joint. Therefore the test proposal 1 is discarded for this investigation but is included as a possible future line work for evaluating this load combination.

The test proposal 2 is then developed and analysed in order reach a final testing model. An iterative process of design and calculation is carried out to define the best shape for the specimens and after several design modifications over this second proposal a final design is reached as depicted in [Fig. 3.2](#). This final assembly design shows a 5 mm plate thickness bolted angular connection with a final set of 45° , 60° and 75° angle variation values.

The bending radius, transition radius and bending clearance distances are justified in the production section in this chapter and the analysis chapter, [chapter 5](#).

The plate's dimensions as well as the assembly specifications for each angle disposition are defined in the drawing collection contained in [Appendix A](#).

The 3D design of the plates is made using the commercial software NX Unigraphics. In order to generate all the design modifications required in the plates to reach the final model, and to generate all the 3D files for the numerical analysis, a parametric design process is developed. This parametric design process is explained in more depth in [Appendix B](#).

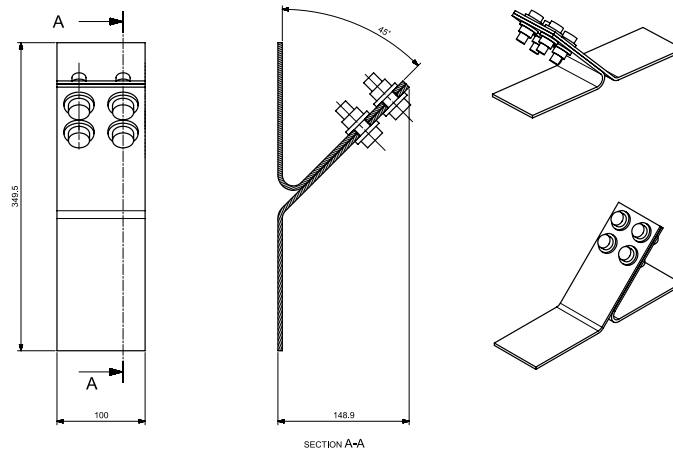


Figure 3.2: Final test design 45° assembly set-up

Design standards application

The plates conforming to this assembly have been designed according to the Eurocode 3 normative: EN 1993-1-8 [3]. This standard gives design guidelines, values, recommendations and alternative procedures for the design of steel structures in its joints connections.

We must outline that the EN 1993-1-8 standard is meant for the design of joints using steel grades: S235, S275, S355 and S460, grades which are under the HSS scope of the project. Although the use of these guidelines is allowed by the EN 1993-1-12 [1] which in its 2.8 section includes the additional rules for the application of the 1993-1-8 [3] standard in HSS.

These standards have been used to define the bolt hole clearances in the steel plates and also in the position of the holes in terms of hole-edge distances and hole-hole distances specified.

Fastener definition

To join the two plates that constitute the test assembly the bolted connection used is the one used on DAF trucks. This connection uses DAF 10.9 Grade flange bolts which are the most used in the joining of the DAF trucks chassis. These bolts are used in order to make the connection similar to a real truck case.

These hexagon head bolts have the peculiarity of having a shank which becomes a smooth dish-shaped flange. This increases the bearing surface and thus decreases the stress concentration in the hole vicinity.

Another advantage in addition to the dish shape bolt head is the closely tolerated contact width of the bolt head which results in a better defined tightening torque and the resulting pre-load scatter.

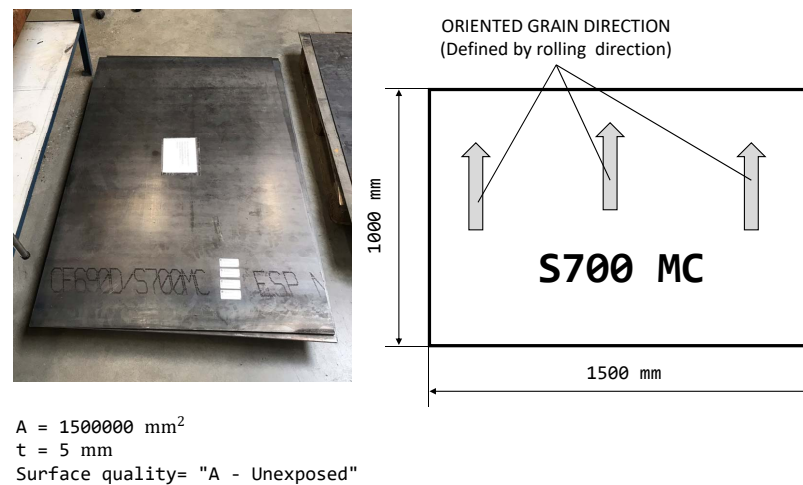


Figure 3.3: Original S700 MC sheet

3.2 Specimen manufacture

Once the design is determined is the moment for the manufacturing process. This process is being carried out by specialist technicians in the university facilities.

The drawings of the pieces and the 3D .dat files for the machine process are provided to the machining staff that uses them to perform the cutting and bending processes from the main material to reach the shape defined for each case.

In the following section the processing methods used for each operation are defined and a follow-up of the specimens through each transformation is done to show the evolution of the test specimens in the process.

3.2.1 Material cutting

The S700 MC bulk metal sheet needs to be cut in correct shape for each angle disposed for the specimens.

To perform this cutting operation a number of different cutting options are available: plasma cutting, laser cutting, oxifuel cutting and water jet among others. So a research is carried out to find which one is the best method taking into account the geometry, precision, number of pieces... and many other parameters in our designs.

To select the most suitable method for our process and material the comparison made by T. Mert [40] for the cutting methods is used. This comparison is displayed in Fig. 3.4 and is possible to extract from among all processes that the abrasive water jet is the winner in the most categories. Due to its advantage of no presenting HAZ zone in the cut material as seen by the ones in plasma and laser cutting, the

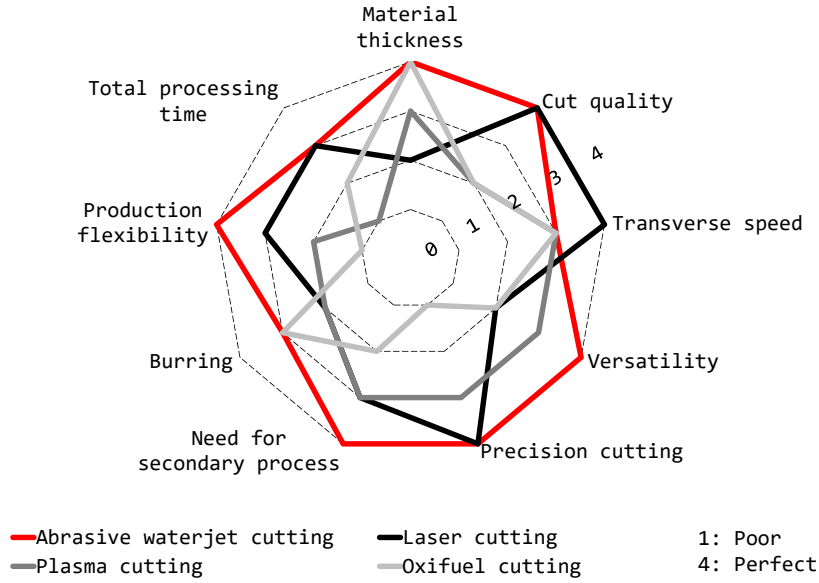


Figure 3.4: Cutting processes comparison

wide thickness range that is possible to operate with, a fair edge quality and a good accuracy with an average of $\pm 0.08\text{mm}$ and up to $\pm 25\mu\text{m}$ makes it the best choice for our case. It is true that the transverse speed is not comparable with the laser cutting but since this fabrication is not intended for a chain production this time increment will not make a decisive difference in the production. This conclusion is also shared by D. Krajcarz [34] in its comparison of waterjet cutting with laser and plasma cutting.

The abrasive used for this operation is rock garnet mesh with grit no:80. This abrasive is determined by a particle size from $212\mu\text{m}$ to $180\mu\text{m}$ and is typically as a waterjet cutting abrasive, sandblasting media, laping, coated or bonded abrasive tools [16]. Garnet chemical composition is compiled in Table 3.1.

$Al_2O_3(\%)$	$SiO_2(\%)$	$Fe_2O_3(\%)$	$TiO_2(\%)$	$CaO(\%)$	$MgO(\%)$	$MnO(\%)$
18.95	40.84	11.20	1.70	10.07	5.99	<0.2

Table 3.1: Garnet 80 mesh chemical composition

The specimens are cut out using the OMAX 55100 JetMachining Center [13] equipped with an OMAX MAXJET 5 Nozzle and a Bulk Abrasive Delivery System that provides the abrasive material to the nozzle to perform the cutting. The pump pressure is defined at 4000 bar for the 5 mm plate thickness.

From the machine display the time, cost, and material quantity are shown for each set of the 3 different angles as shown in Table 3.2.

¹Total of 6 plates, 2 each angle disposition

Cutting process details		
Estimated time for path	44.913	min
Estimated cost for path	18.71	€
Estimated abrasive needed	11.11	kg

Table 3.2: Process details for a group of plates of $\angle 45^\circ$, $\angle 60^\circ$ and $\angle 75^\circ$ ¹

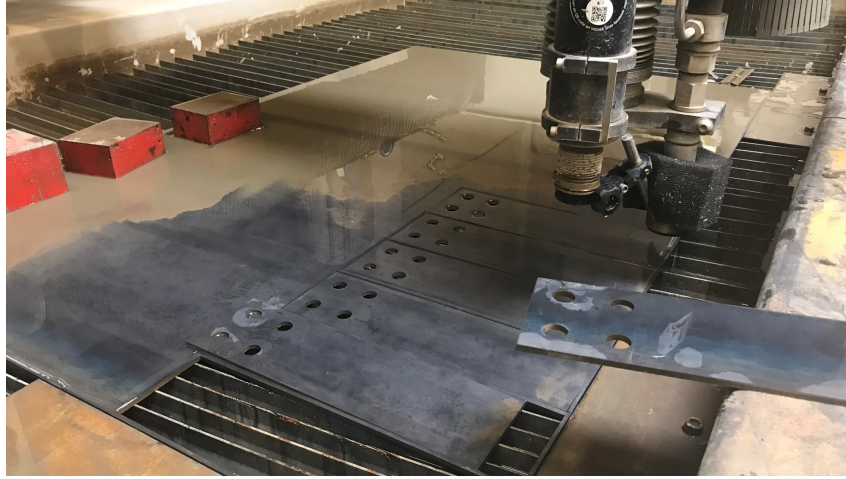


Figure 3.5: Pieces cut with water jet machine

Finally it is necessary to stand out the cutting direction definition from the sheet metal. The rolled direction has to be taken in account due to the fact that the plate's grain direction comes from the mill's rolling process so the grains run parallel to the rolling direction this determines the bending direction so when bending perpendicular to the rolling direction the grain rearranges and shows no effect on the part strength, whereas if the bending is performed parallel to the rolling direction there is a high chance of crack appearance due to the destruction of the grain structure.

Because of the facts mentioned above the longitudinal cutting direction is defined parallel to the rolling direction so the bending process is performed perpendicular to the grain direction. This can be seen in [Fig. 3.6](#).

3.2.2 Bending process

Once the material has been cut from the metal sheet and it is verified that the dimensions are within tolerances the plates are bent with the specified angle: 45° , 60° and 75° in each case.

The machine used for this operation is the LVD PPEB 80 press brake [19] with a 90 Ton pressing force. This machine uses the .sat 3D files of the plate design to bend the samples in the appropriate angle. Due to the sharp angles of 45 and 60 a new dye needs to be produced and included into the bending machine to start with the process.

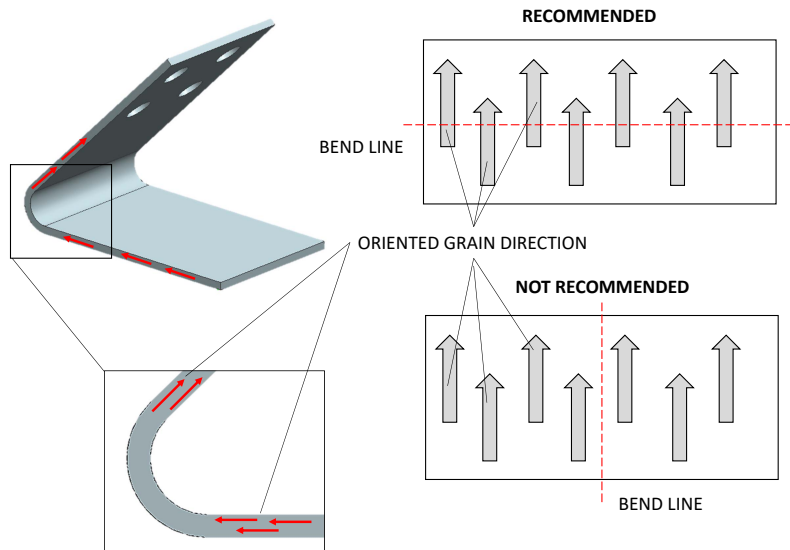


Figure 3.6: Bending parameters definition

The bending radii is a determining factor when sheet metal bending, the steel manufacturer [41] recommends a mandrel diameter of at least 2 x the plate thickness according to EN 10149-2:2013 [15]. This means a minimum bending radius of the plate thickness or 5mm for bends until 180° in S700 MC steel sheets.

The bending process used in our samples is called V- bending. For this bending process the die and the punch are "V" shaped and the bending process consist in the punch pushing the sheet in to the "V" shaped groove in the V-die, causing it to bend.

The air bending process is the one used for the production of the plate set due to its high flexibility. In this process the different bend angles can be obtained using the same tool set since the bend angle is formed by driving the punch into the sheet metal to a specific position within the die opening. This is very convenient since only one die needs to be produced for all the bending angle variations.

The radii defined for this pieces is determined according to the steel metal manufacturer definition and normative exposed in the previous paragraph and the warehouse equipment. That is the reason to use a ball end of $\varnothing 25\text{mm}$ in the press brake punch tip, so an inner radius of 12.5 mm is defined to do the bending. The final plate radius is therefore 2.5 x plate thickness so no stress concentration or bending cracks are expected in the material.

After the bending process when the load application by the punch is released the material experiences an elastically driven change of shape. This recovering in deformation is referred to as springback. R.H. Wagoner et al.[66] determines that the rigid (i.e., no elastic strains), perfectly plastic (no strain hardening) material model defines is sufficient to define springback prediction Eq. (3.1). This simplified model for springback deduction based in Rigid, Perfectly Plastic Result is also shared by [23],[11].

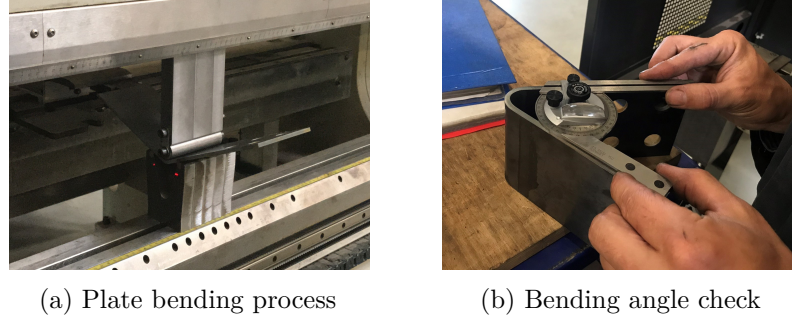


Figure 3.7: Bending process

From [66] is also extracted how the principal material properties affect to the springback in the sheet metal bending:

- Springback is proportional to strength stiffness, that is, σ'_y/E'
- Springback is inversely proportional to sheet thickness

$$\frac{1}{R} - \frac{1}{r} = \frac{3\sigma'_y}{E't} \rightarrow \frac{R}{r} = 1 - \frac{3\sigma'_y R}{E't} \quad (3.1)$$

From the calculations using Eq. (3.1) a minor springback radius value is obtained so no further modifications needs to be done in the bending machine parameters, being this value corrected in the in the checks carried out after bending.

Some repeatability issues have been observed in the plate bending to reach the same angle value in each angle group of the pieces collection. This error comes from the material imperfections and has been reduced by an after bending checking and correction, reducing it to a $\pm 0.5^\circ$ values between plates with the same angle disposition.

As mentioned in the previous section the bending process is performed in a direction perpendicular to the rolling direction so the grain structure of the sheet metal can be rearranged after the bending and minimum residual stresses are implied in the piece as it can be seen in Fig. 3.6. The whole bending process is depicted in Fig. 3.7.

3.2.3 Abrasive blasting

As it is described in [14] the sandblasting is the act of propelling very fine particles of an abrasive material at high velocity toward a surface in order to clean or etch it.

This process is used in order to remove oxide layers, coating or any other debris from the metal surface by a successive impact of grits surface, resulting in an extremely smooth surface.

The impact of the grits against the object's surface inserts compressive stresses in the material. This effects over the treated materials have been studied by E.T. Akinlabi et al [4] in the investigation of the influence of sand blasting on formed

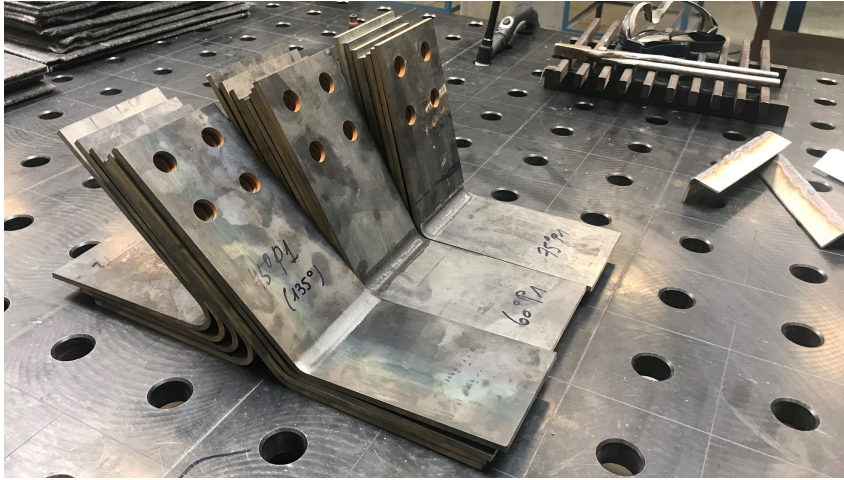


Figure 3.8: Plates produced

mild steel samples concluded that the sandblasting process causes an increase in the Vickers microhardness which also led to an increase in the UTS in the treated specimens. Sand blasted materials have improved properties than the non-sand blasted materials. M. Vasco et al. [64] also determines from the study of reinforcing B500C steel bars that the sandblasting method is a cheap and easily accessible procedure with positive effects on both corrosion and fatigue resistance. Not much research has been carried out about the effects of the sandblasting process in HSS samples.

The sandblasting process defined for the project specimens is air driven, which is preferred rather than the water-driven since it avoids water intrusion into the surface. To perform the treatment a Straaltechniek International sand blasting cabinet [46] is used.

A sandblasting setup is usually composed by the abrasive material, an air compressor and a blaster nozzle. The working principle is easy, a suction blast system uses the compressed air to create vacuum in a chamber (known as the blast gun) The negative pressure pulls abrasive into the blast gun where the compressed air directs the abrasive through a blast nozzle. The mixture is then blown through the nozzle towards the surface of the workpiece. The sandblasting process, cabinet and final result compared with a non treated plate are displayed in Fig. 3.9

The abrasive material used for the sandblasting process is the Garnet 80, same material used for the waterjet cutting and which chemical composition is compiled in Table 3.1.

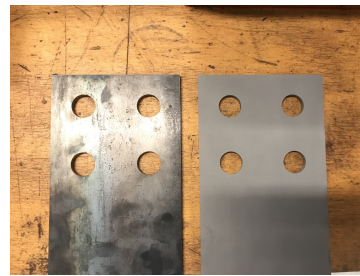
3.3 Assembly

Once all the fabrication process is finished the plates are ready to be assembled. The HSS plates are joined using the DAF bolt and nut fasteners, to do so the plates are aligned and the bolts are positioned.

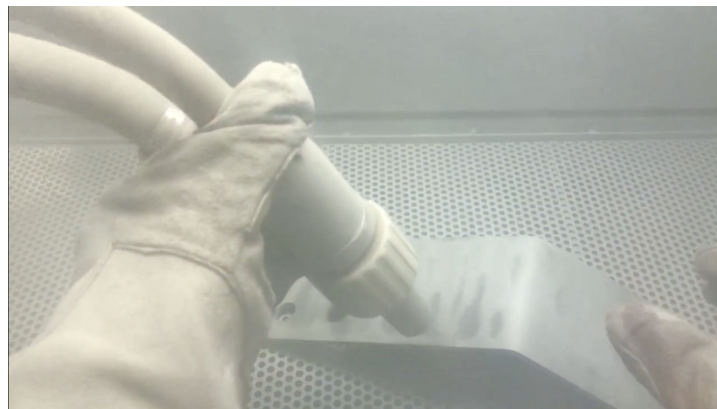
3. SPECIMENS DESIGN AND MANUFACTURE



(a) Sandblasting cabinet



(b) Sheet metal as rolled (left) and after sandblasting treatment (right)



(c) Sandblasting performance

Figure 3.9: Sandblasting process

The torque will define the preload bolt force in the assembly and is critical to correctly define this value.

The torque defined for the test specimens as indicated in the assembly drawings is the one defined by DAF for the A class bolted connections $260 \text{ Nm} + 30^\circ$. were fastened together by applying a preload force to the bolt with an electronic torque wrench with an accuracy of $\pm 2\%$.

Once the torque is applied for each bolt and the data is stored the assemblies are ready to start the test

To reduce the variability in the testing between specimens the same mounting definition is defined for all the samples with the bolt head facing downwards. Also the same fastening operation is performed in all the samples, fixing the bolt head to with a wrench and applying the toque to the nut.

3.4 Conclusion

This chapter introduces the complex joint specimen design representative of the bending and shear combined loading conditions. The design proposals are compiled and a final design is reached. The design integrity is also validated by the European standards used in the design.

The production process of the designs are explained step by step while justifying the production methods chosen for each stage of it. The manufactured parts are ready to be tested in [chapter 6](#).

Chapter 4

Failure modes

This chapter sets out the fatigue failure criteria to be used in the numerical analysis over the project specimens. This criteria is applied to define the crack nucleation as well as to determine the plate's fatigue life.

4.1 Multiaxial fatigue criteria

Since the samples designed in the project are determined to be subjected under shear and bending alternating stresses a multi-axial fatigue state occurs in the plate's contact area.

This complex state of loads means that the application of conventional criteria for predicting fatigue life is not entirely appropriate and the use of multi-axial fatigue criteria is therefore proposed to predict the fatigue life of the samples as it is proposed by [36] and [42].

The multiaxial criteria have different approaches but for the analysis carried out in our project the critical plane approach is used. This approach as it is described in [56] attempts to reflect the physical nature of fatigue damage in their formulation and is based on the fatigue cracks initiation and growth. This crack process occurs within the material on certain planes being the growth and orientation dependent on the stresses and strains on these planes. The critical plane is therefore defined as the plane where a combination of stress or strain components is maximal.

For this study two multi-axial fatigue criteria based on the critical plane approach are used and compared for the fatigue life estimation of the joints.

4.1.1 Smith-Watson-Topper

Smith et al. [53] proposed a simple form of a damage parameter, SWT, described as stress and strain product for fatigue life determination.

This criteria defines the critical plane as the plane where the product of the the maximum normal stress (σ_1^{max}) and the maximal strain range (ε_1) throughout one load cycle are maximal as it is shown in Eq. (4.1).

$$SWT = \left(\sigma_1^{max} \frac{\Delta \varepsilon_1}{2} \right)_{max} \quad (4.1)$$

The SWT parameter considers both elastic (HCF) and plastic (LCF) strain components but since the loads defined in this project are defined for HCF the plastic term in the equation can be discarded for our case study.

4.1.2 Fatemi-Socie criterion

The Fatemi- Socie criteria [18] determines the critical plane as the one with the maximum shear strain amplitude ($\frac{\Delta \gamma_{max}}{2}$) and the maximum normal stress ($\sigma_{n,max}$) acting on the maximum shear strain amplitude plane. The equation is illustrated in Eq. (4.2).

$$FS = \frac{\Delta \gamma_{max}}{2} \left(1 + k \frac{\sigma_{n,max}}{\sigma_y} \right) \quad (4.2)$$

4.2 Criteria application

Both failure modes criteria are applied in the [chapter 5](#) in order to determine the crack initiation localization and the fatigue life cycles.

The application of these failure methods is performed through python scripts executed from the Abaqus interface. This script extracts the numerical results from each element/node recursively in all the steps and defines a contour plot in the analysis surface.

Since the scrip definition is out of the scope of the project these scripts have been provided by the research department. For this reason, only the results obtained from the application of this files will be evaluated.

4.3 Conclusion

This chapter introduces the multi-axial fatigue criteria for the crack nucleation and propagation calculation for the numerical approach.

Two different critical plane approaches are defined in order to investigate a correlation between those approaches results and the testing failures observed.

Chapter 5

Analysis and evaluation of the results

The finite element method is used in this project in order to calculate the stresses, strains, fatigue behaviour and contact behaviour of the model. The FEA analysis gives us a simulation of the behaviour of the model and empowers the creator to do further changes on it before the manufacture which saves a lot of time and resources. For the analysis of the assemblies the commercial software Abaqus CAE is used in order to define the simulations and extract the results.

This chapter presents the definition of the finite element model, establishes the numerical criteria on which the analysis is carried out and sets out the results obtained from the simulation so that they can be compared with the test results with the aim of validating the numerical model.

5.1 General meshing parameters

In order to define the meshing for our specimen some assumptions have been taken into account. The element type used is C3D8R linear brick elements with reduced integration. The computational time for the analysis is reduced by only defining half of the symmetry and imposing conditions for a symmetry along the YZ PLANE

Both plates are put into contact with a surface to surface contact pair with a finite sliding formulation with a penalty iteration property for the tangential behaviour defined as the friction coefficient for the plate-plate interaction.

Nut and bolt head surfaces in contact with the plate are also defined as a contact pair in the same way as the plate-plate contact and a last condition is imposed for the contact between the bolt shank and the plate hole in case the sliding is enough to enable this contact.

The indications described by R. J. Tyrrell [61] for obtaining converged solutions in Abaqus contact simulations have been used in the definition of the contact parameters through all the analysis definition process.

The quality of the surface mesh has to be good to get acceptable finite element results. Element quality for quadrilateral element is defined by two factors:

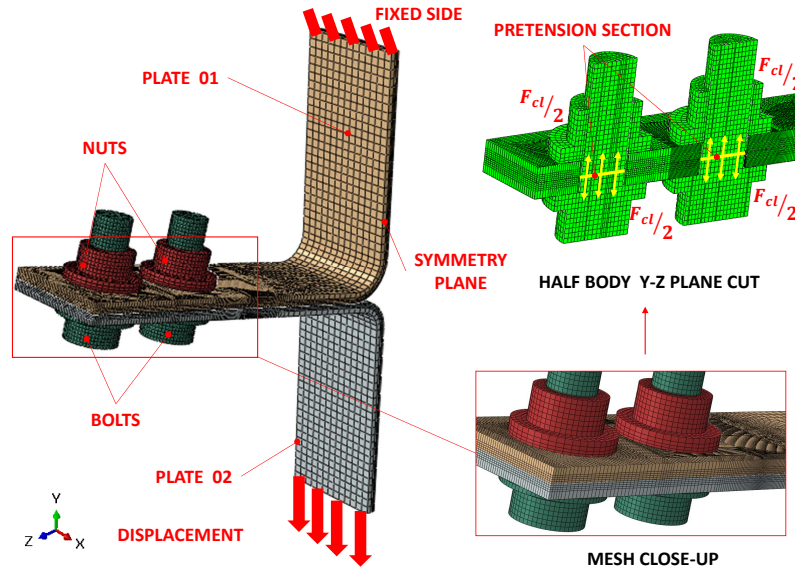


Figure 5.1: FEM of the plate assembly

1. Distortion factor
2. Aspect ratio

The **distortion factor** represent the quadrilateral internal angles maximum deformation values for each element. Depending on the authors different values for the distortion factor are adopted for each mesh definition. In this project the value adopted is determined for quadrilateral internal angles falling within 90 ± 52.5 , value determined and adopted by SH Lo and CK Lee [37] and shared by Tohura et al. [60] in their study.

The **aspect ratio** is defined as the relationship between the largest to the smallest length of the sides of the element. The best value for the ratio is 1 so the aim is to keep that value as close as possible to this value.

The distortion factor and aspect ratio in our plates are kept within the specified values for the contact zone mesh in order to assure the numerical model accuracy. In this study any element surpassing this range is considered unacceptable and a re meshing is made.

Three steps are defined for this simulation:

1. Initial step : All the contact iterations and boundary conditions necessary for the model are defined in this step.
2. Bolt load: The preload force is applied in a ramp amplitude for each bolt in the assembly
3. Axial load: The load force is imposed to the structure as a displacement condition defined for the lower plate.

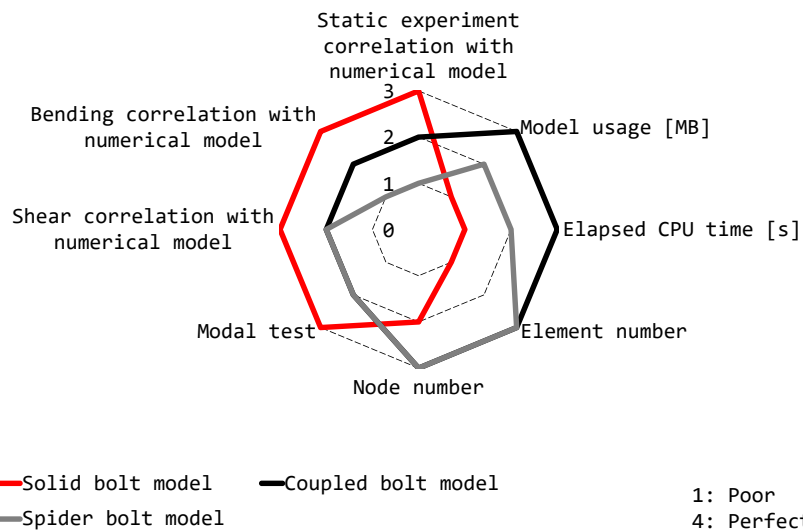


Figure 5.2: Finite element models for a bolted joint

Symmetry boundary condition is applied to the plate side since the simulation works with a simplified model in order to reduce simulation time and the plate symmetrical part has been removed

The analysis job is submitted to the university server that runs the .inp files. This server uses a 12 core 32 GB RAM @1.9 GHz computer to perform the simulation and retrieves the .odb file.

5.1.1 Fastener numerical model

To model the bolted connection there are a few ways to proceed. KIm et al. [32] research shows a comparison between the different finite element models for the bolts. The comparison results are extracted in Fig. 5.2 and from them we can extract that among the finite element bolt models the solid bolt mode despite having the longest computational time and the highest model usage which lead to higher resources usage have the highest correlation with the experimental set-up, being this accuracy within the experiment more noticeable in the area near the bolt hole.

Therefore the solid bolt model approach is used in this project for the joint FEA analysis. For this model an intermediate section needs to be defined in the plane between the two plates in order to define the bolt load applied.

5.2 Mesh convergence

As a starting point to validate and get reliable results in the analysis a mesh convergence study is being carried out in order to select an appropriate mesh size

for the assembly. The mesh convergence study allows to define the mesh size that achieves accurate calculation results in an acceptable computation time.

To do this the mesh in the contact zone has been refined in by $50\mu m$ steps until a value of $300\mu m$. Then the maximal principal stress values along a path tangential to the bolt circle are plotted for each element size.

The aim of this study is to get an independence in the study form the mesh size so when the maximal principal stress magnitude difference between two consecutive values is to be under 2% as it is used by [28] and [31] the mesh is considered to be independent from the calculations and the mesh size previous to the last mesh value where the criteria is satisfied is used.

In the Fig. 5.3 normalized tension values are plotted in the contact zone. From the results we can derive an optimal mesh size of 0.35×0.65 can be adopted for our study.

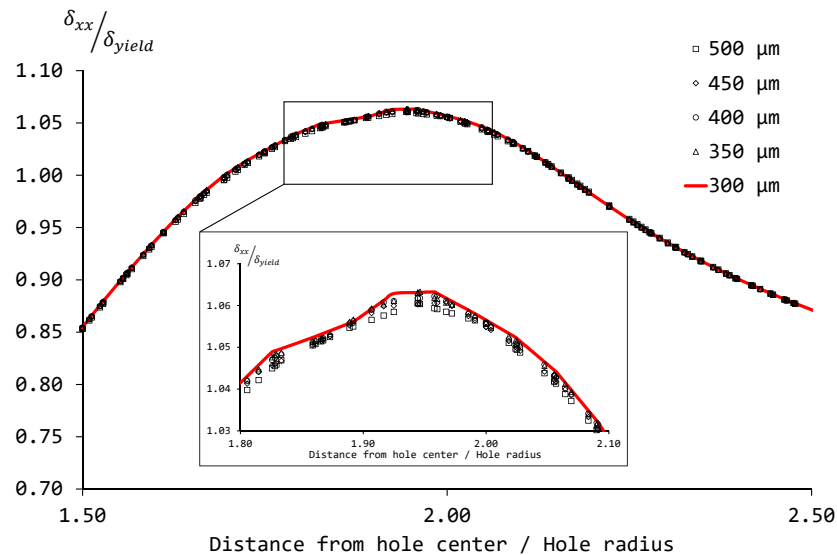


Figure 5.3: Normalized maximum principal stress stress distribution along the normalized centreline of the specimen for different mesh sizes

Fig. 5.4 shows the exponential relationship between the mesh size and the calculation time and displays the dimensional maximum principal stress value in correlation with the mesh size to corroborate the mesh convergence analysis since this curve slope stabilises in the $350\mu m$ contact mesh size.

5.3 Numerical calculations

The results obtained from the numerical analysis are used to define the design characteristics and to determine the load distributions for the test.

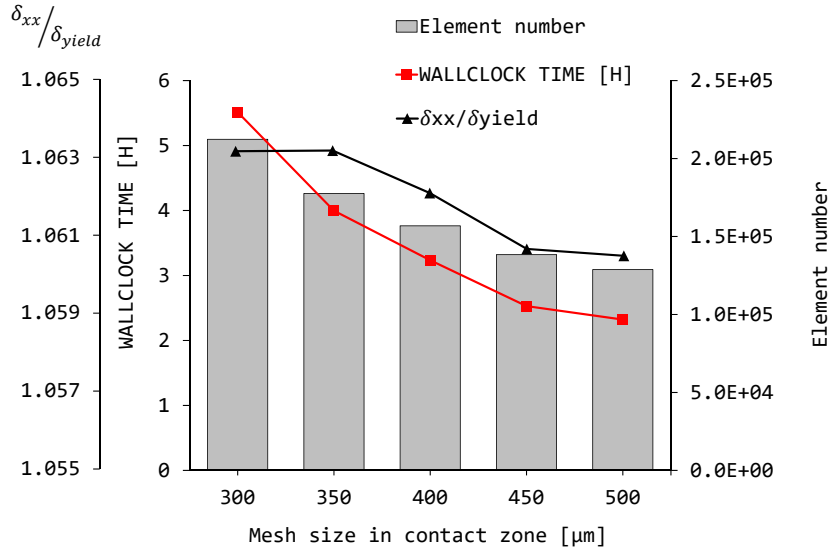


Figure 5.4: Calculation time and element number of the overall assembly for each mesh size in the contact zone

The 3 specimen angle dispositions are analysed and compared. A displacement is imposed in the lower plate and the stress, strain, shear, c shear and c slip variables are studied. The displacement condition in the analysis is preferred rather than a load ramp due to generate more stable solutions in a shorter computational time and presents less convergence issues in contact analysis.

Since the numerical model is defined imposing a displacement value as a load application the reaction forces are also determined in order to translate the numerical analysis to the testing machine loading conditions. The reaction moment in the upper plate is also determined for each load condition to determine the bending moment magnitude induced in the testing machine once the specified load for each analysis is applied.

From Fig. 5.6 it is demonstrated that as the angle becomes sharper there is an increase in the shear stress in the plates. This statement validates the design approach from chapter 3 as the load conditions can be determined by a parameter modification which is the angle variation.

The contact slip increases in the same way as the shear stress Fig. 5.7. Both values are correlated and validate the design approach.

Both shear stress and contact slip incrementation values determine that with the angle sharpening a sliding value leading to a small fretting condition is possible.

Even though the shear values in the plates are demonstrated to increase with the angle sharpening its magnitude is not determinant for the plate fracture since the maximum principal stress modulus Fig. 5.5 caused by the bending moment in the bolt flange is decisive for the failure and its location coincides with the fatigue criteria crack initiation determined in Fig. 5.11.

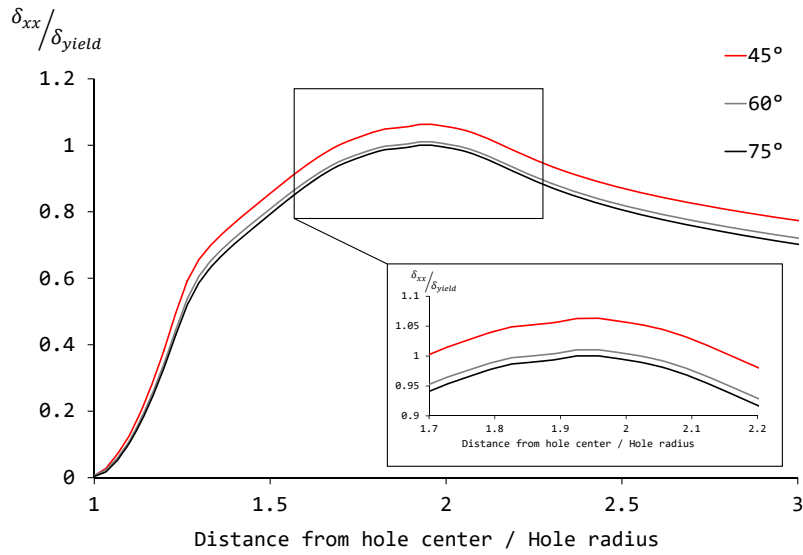


Figure 5.5: Normalized maximum principal stress distribution along the normalized centreline of the specimen for the different bend angles

The Fig. 5.8 presents the contact status and contact shear for the 60° plate configuration. As is it mentioned before the shear stress is minimum in the plates and therefore a marginal slipping value is to be expected in the hole vicinity. This determines that a minimal fretting value can be expected but a fretting fatigue behaviour is not expected for this plate configurations.

It is shown that the contact pressure Fig. 5.8b is the same for the different angular variations. This is caused by the fact that this value is defined by the pre-load applied to the union screws, which is the same for all specimens.

Agreement radius analysis

Since it is proposed in the design stage to include an agreement radius in order to ensure a smooth stress flow different radii values have been tested and along with with a no radius plate model design.

Form Fig. 5.9 is obtained that no major significance in the maximum principal stress point is obtained, being the no bend stress transition values similar to a sharp agreement radius. This fact combined with manufacturing complexity that the agreement radius involves, and also the tight of the design dimensions to fit in the testing machine this agreement radius is discarded so the final specimens will not present this feature.

A ~25% weight reduction is obtained from the removal of this feature with the consequent saving of material that this entails.

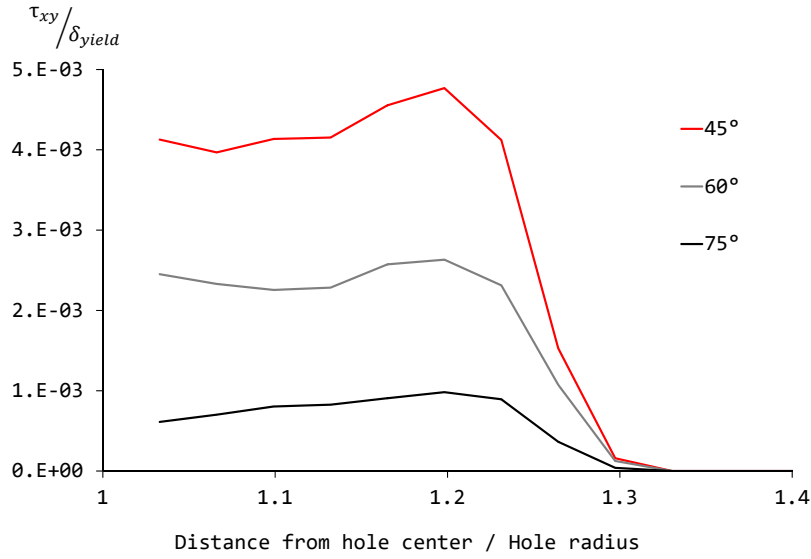


Figure 5.6: Normalized shear stress distribution along the normalized centreline of the specimen for the different bend angles

5.3.1 Fatigue criteria application

To determine the fatigue crack initiation and life SWT and Fatemi socie multi-axial fatigue criteria defined in [chapter 4](#) are applied in the models.

A correlation is found between this two fatigue criteria methods since both of them predict the crack origination is in the same area for each angle definition as it can be seen from the numerical results are compiled in [Fig. 5.11](#).

The fracture crack initiation is determined to be at a normalised distance of ~ 1.95 Distance from hole center / hole radius. This value is true for all the specimens and is correlated with the test model. This validates the the fatigue criteria methods and will be assured with the test specimens in [chapter 6](#).

From this criteria the approximate life cycles for each specimen and load condition is obtained so [\[45\]](#) defines the difference between LCF and HCF in $N = 10^3$ So all the test developed in this project are determined therefore for cycle values in the HCF.

Both criteria are correlated in [Fig. 5.10](#). This chart shows the both fatigue failure in a transversal path from the hole center, defining the same crack initiation point for a set of load steps.

Since both [Fig. 5.10](#) and [Fig. 5.11](#) present a high correspondence in the fatigue cracking prediction the life cycle and the theoretical S-N curves for the samples are elaborated applying only the SWT criterion.

The S-N theoretical curves for the fatigue life in the samples are displayed in the [chapter 6](#) under [Fig. 6.7](#)

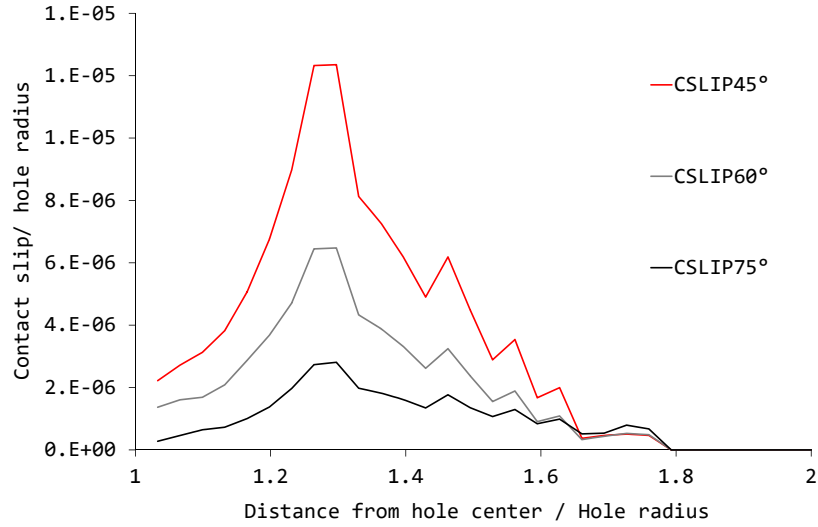


Figure 5.7: Normalized contact slip along the normalized centreline of the specimen for the different bend angles

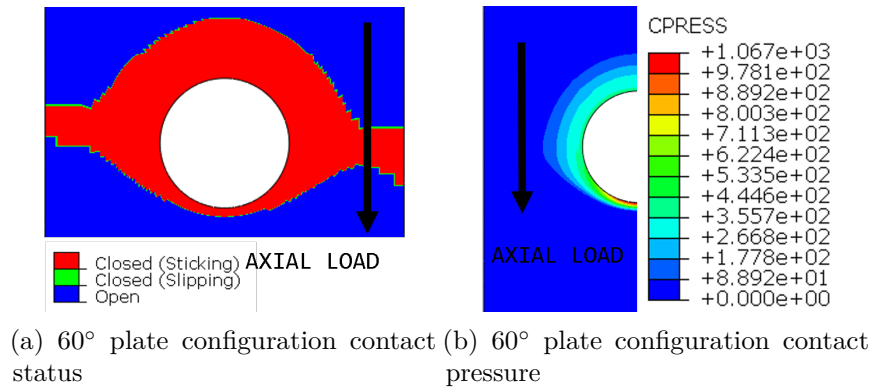


Figure 5.8: Contact pressure and contact status contour plots for the 60° plate configuration

5.4 Conclusion

In this chapter the numerical results for the FEM model are exposed to justify the design decisions and to determine the numerical values to be verified in the testing process.

From the results it can be extracted that the peeling effort is the determinant failure method since the shear stress and contact slip values are not critical for the failure in the angle dispositions studied. However the angle variation does have a significant effect in the shear and slipping values, and since the angle sharpening reaches higher values this stress loads could have a determinant effect in the failure

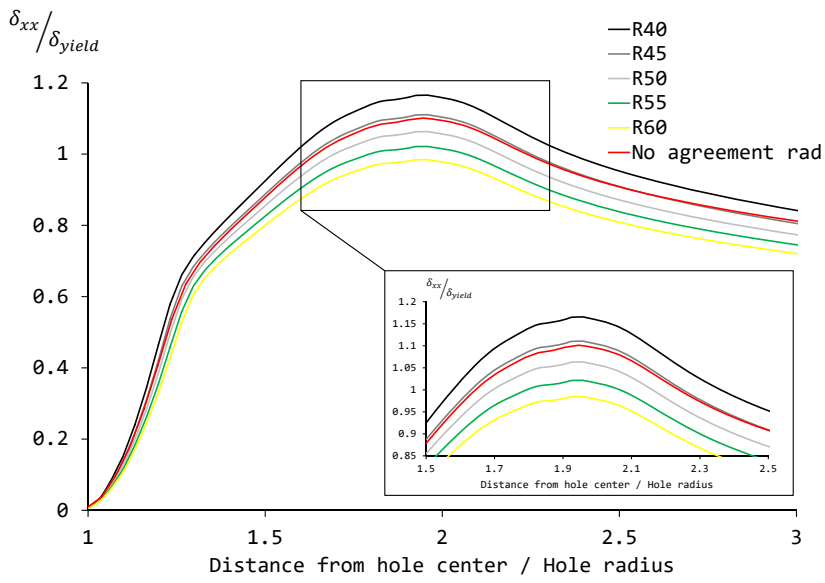


Figure 5.9: Rad agreement tension transition

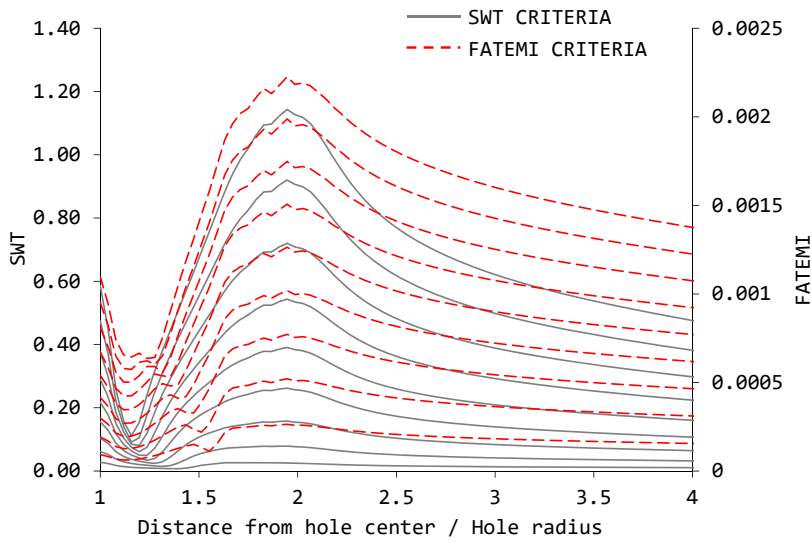


Figure 5.10: Fatemi-SWT correlation for the 45° plate assembly

mode. This supposition is proposed as a future line work to continue the combined load plate bolted connection research.

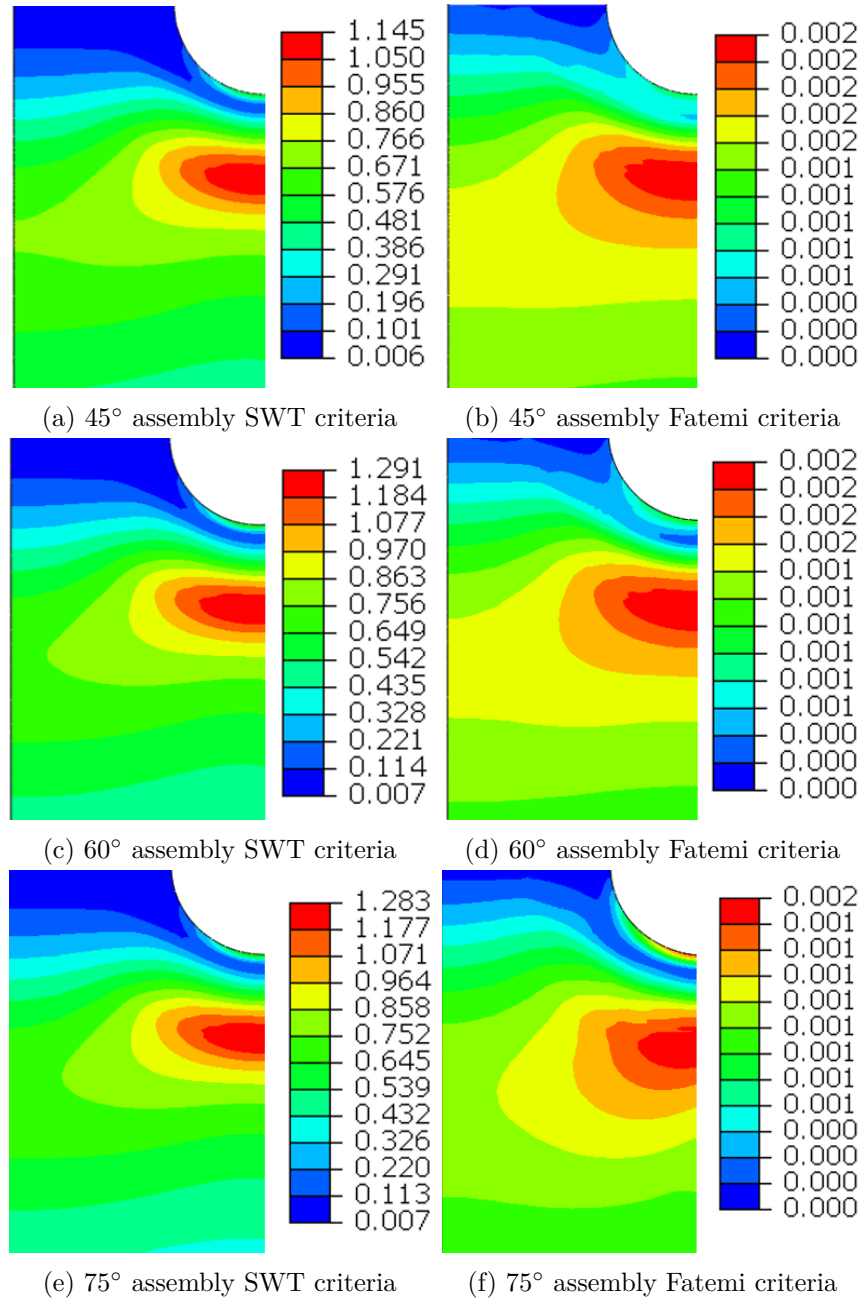


Figure 5.11: Fatigue criteria application for each case

Chapter 6

Testing procedure

Once the loads are identified, the geometries are numerically calculated and the final drawings released for the production the process of testing starts.

A fatigue test is carried out in the specimens in order to analyse the nature of the failure and reach a correlation within the test and the numerical models.

6.1 Test set-up

The bolted assemblies are tested with a Zwick HA100 servo-hydraulic load frame [70],[71] with a maximal axial load of 100 kN.

Two types of testing approach are defined to carry out in the plates:

1. Same axial load for all specimens (Same cyclic load amplitude)
2. Same maximal principal stress magnitude in the fracture area

Test approach / Specimens	45°	60°	75°
Same axial load	6.00 kN @10 Hz	6.00 kN @10 Hz	6.00 kN @10 Hz
Same stress magnitude	6.00 kN @10 Hz	4.85 kN @10 Hz	4.4 kN @10 Hz

Table 6.1: Test approaches

The parameters are adjusted for the desired testing conditions. The load ratio is kept constant at $R_s=0.1$ so that the specimen is only subjected under traction axial loads. The frequency for all the tests is set to a value of $f=10$ Hz. The frequency is kept constant at this value during all the test due to the bolt position in the plate that induces a reaction moment into the machine load cell leads to instabilities in higher frequency values are reached during the testing.

6.2 Correlation with the numerical model (DIC)

In order to validate the numerical model with the test a DIC stereo installation is positioned in front of the the testing machine to get a set of images that will be interpreted by the MatchID Stereo program [39]. The DIC arrangement consist in two digital cameras mounted on a tripod positioned at a 45.4 cm distance from the plate and the camera's relative angle is kept at 20.1°. This cameras have a lens with a 25mm focal length and a resolution of 2752x2206 pixels. An halogen lamp is mounted behind the cameras to improve lightning and contrast and minimize the pixel saturation in the images.

The cameras are focused toward the thickness of the plate since the specimen thickness is determined to be the detection area and is completely covered with a speckle pattern to perform the image correlation process.

To obtain a correlation between the numerical and the experimental model the DIC method is used during the testing. The testing model is subjected to a series of static load from the resting value (0 kN) to a final 6 kN value in 1 kN step values. Two sets of images are taken, firstly one is done prior applying the static loads and then a second one is carried out after 20000 cycles so the friction coefficient is stable and the specimen behaviour is considered to be consistent. Images of each step increment are recorded and stored to be treated with the MatchID softwate.

Values are stored for $[U_1, V_1, W_1]$ displacements in the upper plate Fig. 6.1a and $[U_2, V_2, W_2]$ for the displacements in the lower part Fig. 6.1b . The difference between the absolute displacement of each plate $[\Delta U, \Delta V, \Delta W]$ represents the relative displacement between the plates and by obtaining the vector magnitude a correlation can bi find between the images and the numerical model. The DIC parameters used for the study can be find in Table 6.2

This displacement vector is then compared against the numerical analysis and a correlation is obtained between those two models with an average error <4% as depicted in Fig. 6.1c

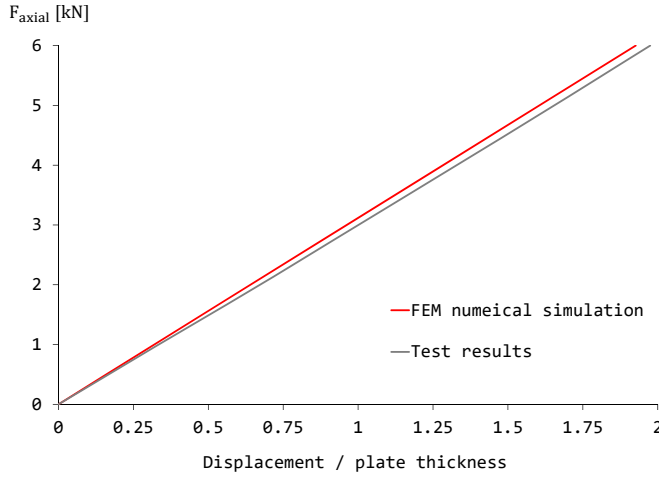
The 75° assembly is used to validate the models and since the correlation is successful the specimens are determined as properly validated.

Parameter	Value
Correlation coefficient	Zero-Normalized SSD
Interpolation order	Bicubic spline
Transformation order	Affine
Subset size [pixels]	21
Step size [pixels]	10
Noise handling	Gaussian
Kernel size	5
History	Spatial

Table 6.2: DIC parameters



(a) Inferior plate DIC detection zone (b) Superior plate DIC detection zone



(c) Comparison between numerical model and test results

Figure 6.1: DIC correlation process

6.3 Results and discussions

From the test performance a dynamic stiffness chart [Fig. 6.2](#) is obtained. This chart shows a big drop stiffness in the first 10^3 . This behaviour indicates the material stabilization in the test and the friction coefficient equilibrium, the material recovers in the incoming cycles and the test is developed around the initial value until the crack initiation. Once the crack has started, it propagates in the material fast until reaching the 20 mm maximum displacement value imposed in the test.

After the testing the plates are examined and studied. When the same load is applied [Fig. 6.3](#) through all of the test specimens different load cycles are determined due to the bending stress concentration in the bolt head. A higher stress concentration is determined in the higher angle plate disposition, which lead to shorter fatigue life.

From the image [Fig. 6.3b](#) the failure mode characteristic of these specimens can be observed. This plate shows fretting marks in the bolt head area and prior to them the initiation of the fracture. This type of failure represents that even though a relative slip is observed between the parts and the surface suffers surface wear, this is not the determining failure load condition. If it were, the crack and the sliding marks would coincide, giving rise to the phenomenon of failure known as fretting fatigue. But being the beginning of the crack at a certain distance it is concluded

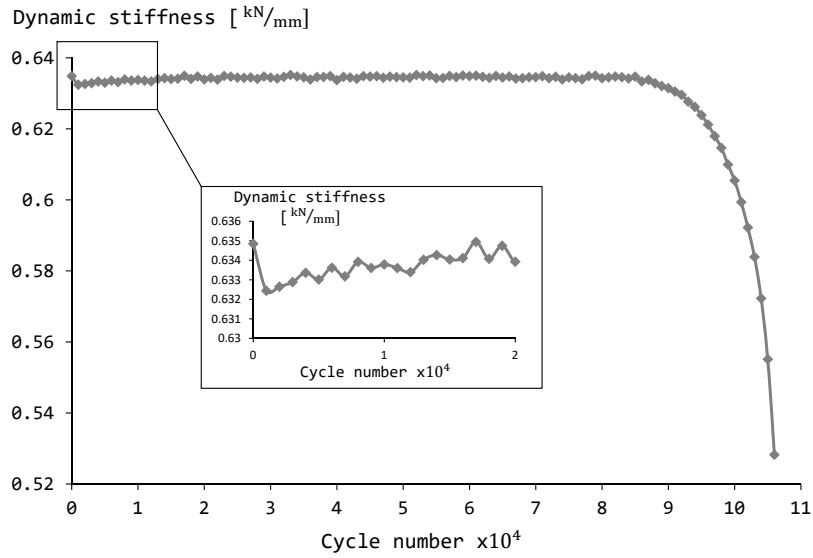
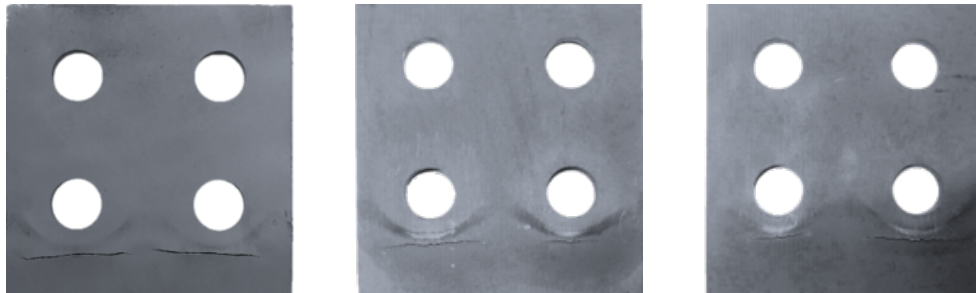


Figure 6.2: Dynamical stiffness behaviour in the tests



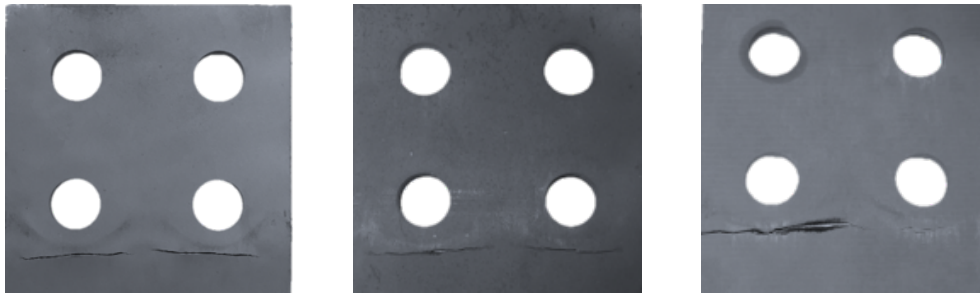
(a) 45° assy fixed axial load (b) 60° assy fixed axial load (c) 75° assy fixed axial load

Figure 6.3: Specimen results for the fixed axial of 6kN load test

that the bending moment caused by the plate peeling is the determining failure mode as predicted in the numerical model. This also corroborates the DAF experiments in the Duramech project, in which, the fracture behaviour is determined by the bolt flange head geometry.

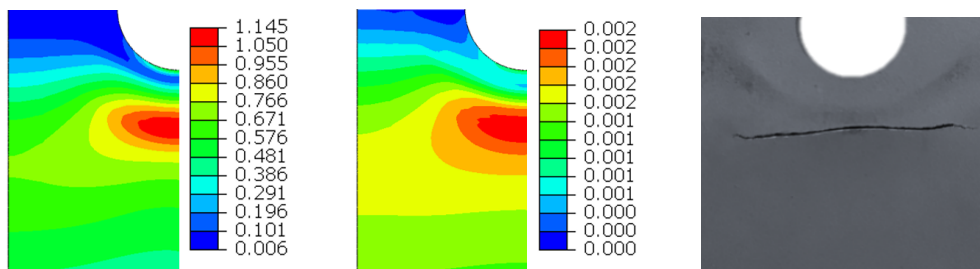
When the specimens are testing at similar maximum principal stress values resembling life cycles are obtained for the specimens. with values over 10^5 cycles. It is observed from the collapsed models in Fig. 6.4 That with the increase in the fatigue cycle life the fretting marks on the plate surface and the crack initiation get closer to each other. This tendency can be clearly observed in the Fig. 6.4c in which the crack initiation and the fretting marks almost overlay each other.

This coincidence in the fretting marks and fissure foundation is interesting since a driving factor to obtain a mixed fretting and bending combined failure mode could be determined by a certain load test specification that present fatigue life closer to



(a) 45° assembly 6kN load (b) 60° assembly 4.85kN load (c) 75° assembly 4.4kN load

Figure 6.4: Specimen results for same maximal principal stress magnitude in the fracture area



(a) 45° assy SWT criteria (b) 45° assy Fatemi criteria (c) 45° assy test result

Figure 6.5: Numerical model correlation with the test

the ones experienced in the Fig. 6.4c. This fact investigation is defined as a future line work.

As it can be seen in Fig. 6.5 an analogy is determined between the numerical analysis and the test results in the fatigue crack determination point and the estimated fatigue life. The numerical model is validated and its results are determined to be a fair failure prediction method.

The 45° assembly is forced to break to check the crack section. The transversal fracture section shows the crack propagation marks which can be follow until the fracture initiation point in the plate contact zone. It is also observable in the figure part with brighter colour which means the ductile fracture in the material.

The process of the fatigue cracking is divided in three stages, in the first one the crack is nucleated, this stage may be short-lived; then the second stage means the crack propagation which involves most of the life of the piece. If the alternating load persists and the crack is sufficiently propagated a sudden fracture of the piece is experienced.

For our test in order to avoid any damage to the test equipment a displacement condition is added so the test stops during the crack propagation stage. The fracture surface is identified in Fig. 6.6.

The test results for the cycle number and the stress amplitude magnitude are compiled in Fig. 6.7. The S-N values of the test experiments are correlated with the

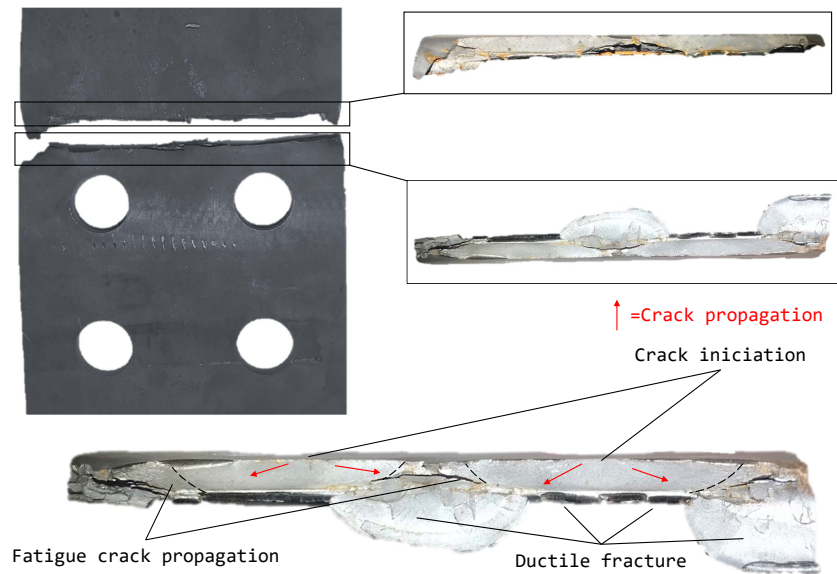


Figure 6.6: Fatigue crack transversal surface identification

theoretical S-N curves calculated in the analytical model.

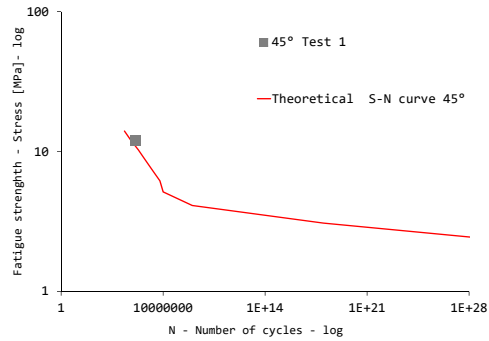
The test values S-N values for each angle disposition are similar to the analytical life curves calculated using the SWT criterion. The analytical life cycle application is therefore validated with the testing models.

6.4 Conclusion

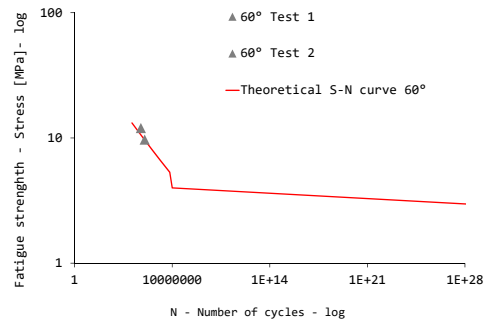
In this section the numerical model is correctly correlated with the tests by the DIC method and the analytical fatigue crack initiation predictions show a match with the testing specimens crack results. This reciprocity in the results is determined to validate the analysis procedure.

From the fracture transversal section shows a fatigue fracture definition from which is possible to identify the fatigue part parameters clearly as is shown in Fig. 6.6

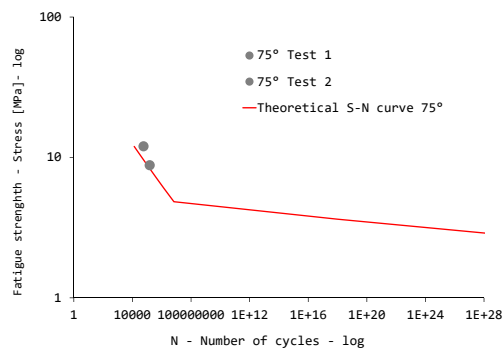
Due to the project tight schedule and the large amount of time it takes to perform the tests a small test range number is performed in this project. It is determined as a future work line a testing continuation to assure the replicability of the obtained testing values and a experimental S-N curve determination in continuation with Fig. 6.7.



(a) S-N theoretical curve and test value for 45° specimen



(b) S-N theoretical curve and test value for 60° specimen



(c) S-N theoretical curve and test value for 75° specimen

Figure 6.7: S-N distribution and theoretical curves for the tested specimens

Chapter 7

Conclusion and future work lines

In this project a bolted connection subjected to a complex load state is defined and tested. From the test and analytical results it is observed that the angle variation does have an influence over the plate tensional behaviour, eventhough the failure mode is set to be determined by the bending efforts rather than the combination of both fretting and bending load cases.

To demonstrate the angle influence on the shear stress and slip conditions for the plates a numerical 30° plate configuration is analysed. From [Fig. 7.3b](#) a 31.31% slip increase is observed and [Fig. 7.3a](#) depicts a 45.05% increment of the normalised shear stress in comparison with the 45° plate configuration.

This increments in the tangential plate's behaviour determine a future line work for this connection with the design and test of sharper angle elements to evaluate the both load conditions.

Since a sharper angle value bolted connection could be difficult to reproduce due to the bolt mounting clearances the test proposal 1 [Fig. 3.1a](#) to [Fig. 3.1c](#) in [chapter 3](#) is taken up again This connection which allows to increase the angular values without any design obstruction, only with the drawback that it requires a testing equipment which allows high plane misalignments between the upper and lower plates and is not available in the facilities of the university. Different equipment or testing approaches could be used over this specimen to corroborate the angular behaviour and compare it with the results obtained in this project.

This complex bolted connection can be used also to corroborate V. Venugopal shell model bolt approach [Fig. 7.1](#). The shell model connection means a high computational time saving analytical procedure, with a time reductions of 90% compared to the full solid model. This drastic reductions in the calculation time are very convenient when working with complex load states such as the one of this project.

Since a a high correlation value has been identified between the analytical model, the DIC metrology and the testing results the the model is validated. This means that the numerical model will show an appropriate behaviour and can be used in

7. CONCLUSION AND FUTURE WORK LINES

other load conditions. The results obtained in this project can be compared with the shell model approaches defined by V. Venugopal in [65] to determine this model approach accuracy against the full solid model.

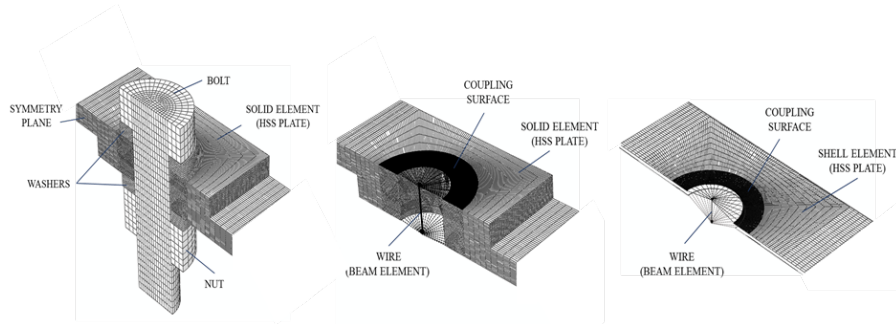


Figure 7.1: V. Venugopa equivalent shell model bolted connection approaches

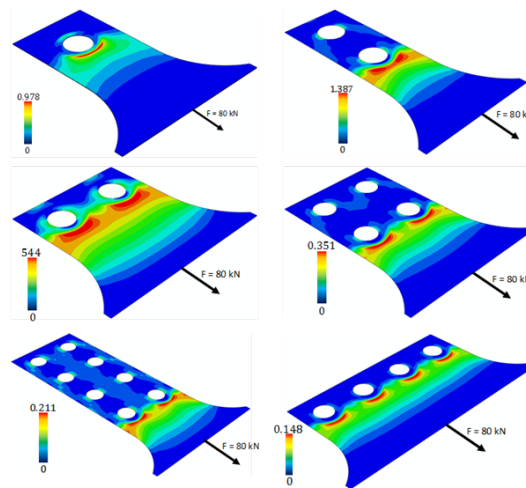
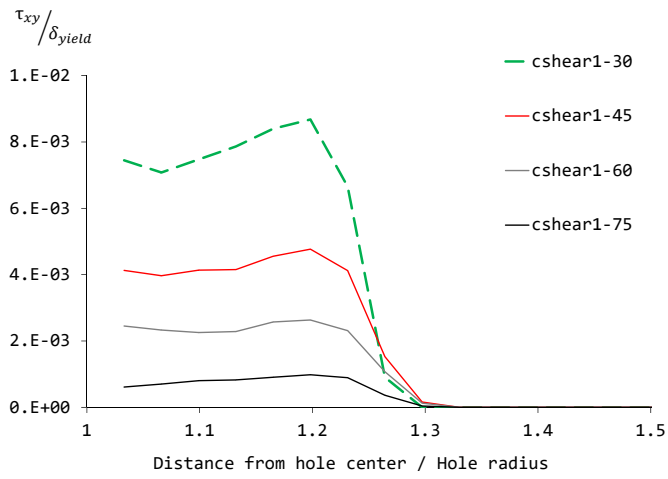
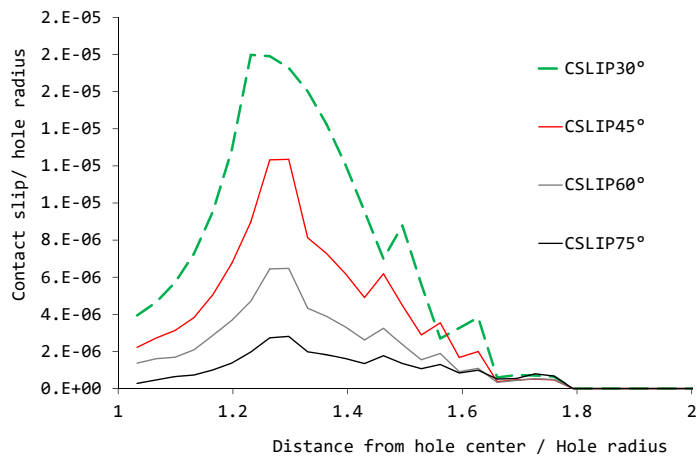


Figure 7.2: V. Venugopal multi-bolt plate analysis with equivalent shell model

In general lines the bolted connection proposed in this project is defined as a starting point for a research in the simultaneous shear and bending fatigue loading conditions and as another load evaluation for the DAF case optimizations.



(a) Contact shear with 30° plate configuration introduction



(b) Contact slip with 30° plate configuration introduction

Figure 7.3: Introduction of a sharper angle value in the plate parameters

Appendices

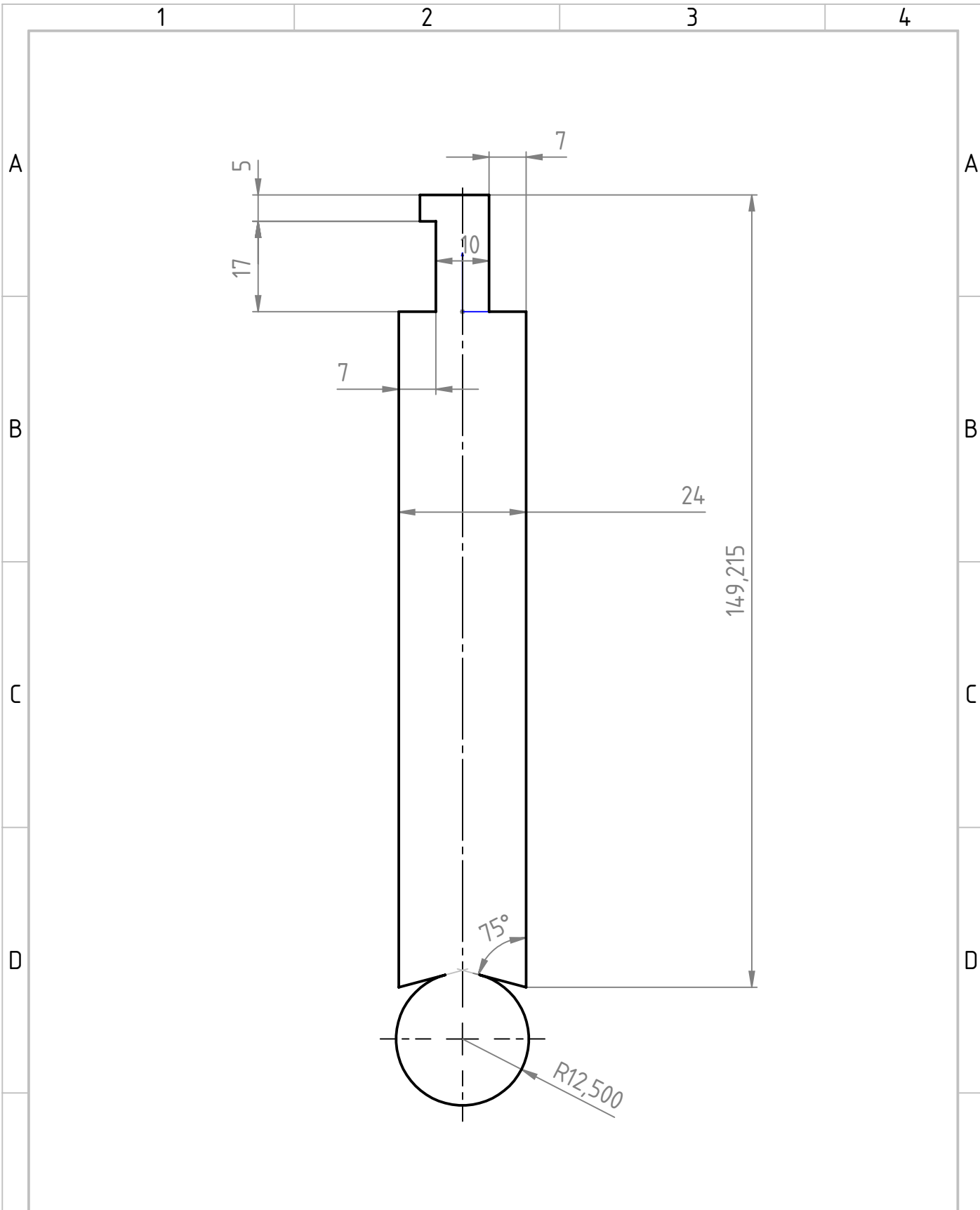
Appendix A

Drawing compilation

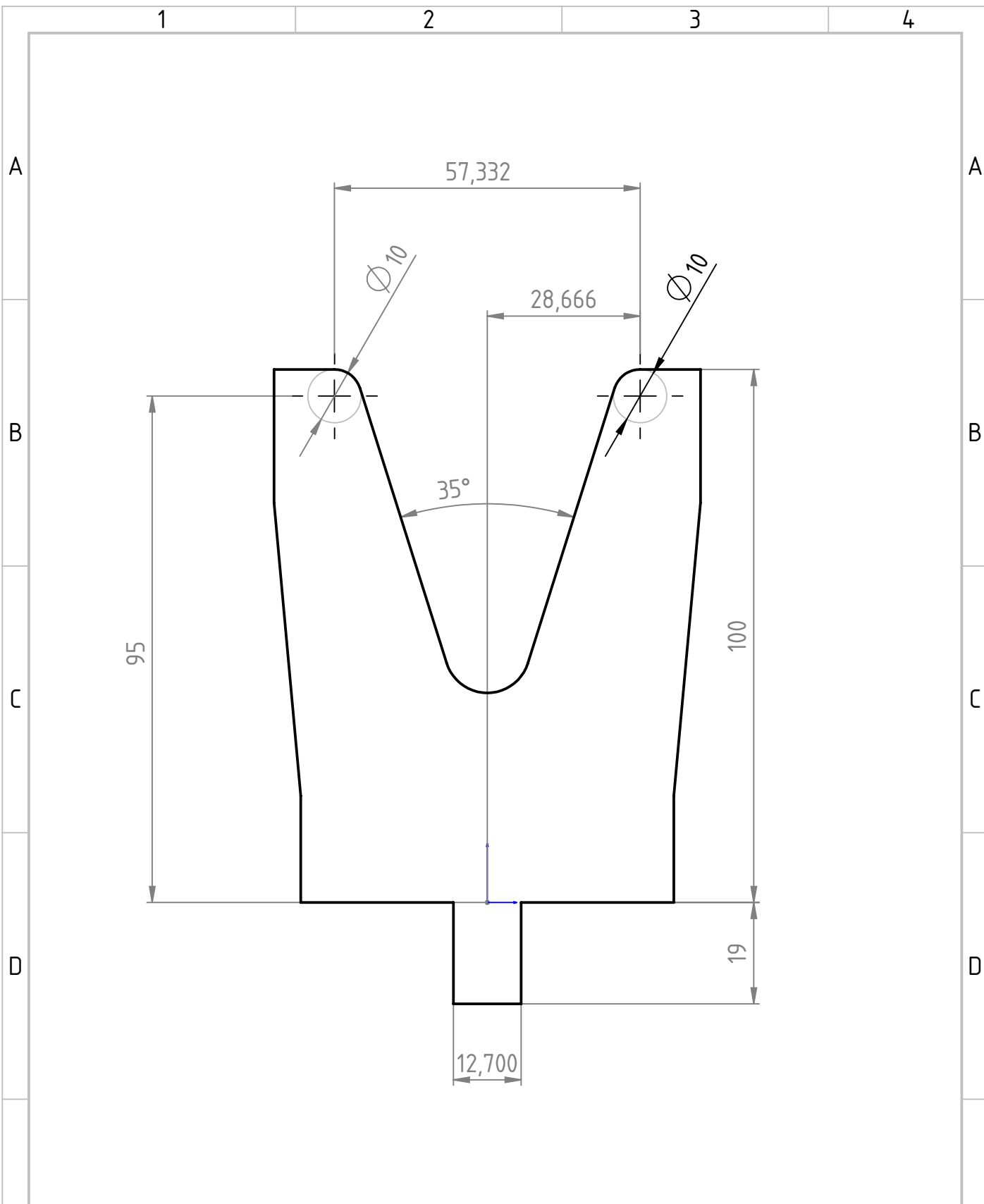
This chapter compiles all the model drawings for production, the assembly mounting drawings and the die and punch purpose-built for this application.


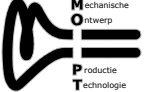
The punch and die are produced by the university personnel so the drawings are provided by them.

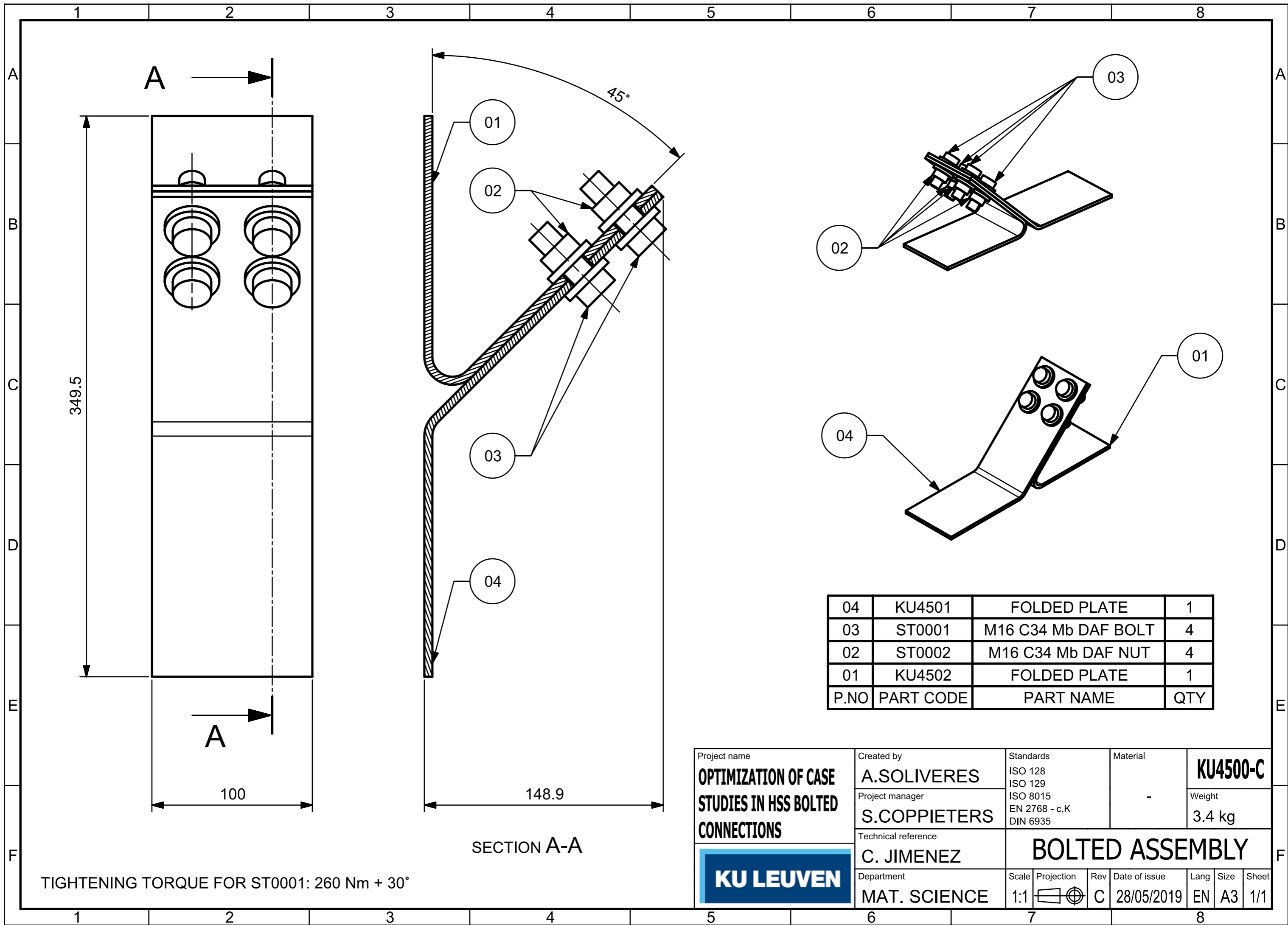
1. Punch drawing page [51](#)
2. Die drawing page [53](#)
3. 45° Plate assembly - KU4500-C page [54](#)
4. 45° Plate 01 - KU4501-C page [55](#)
5. 45° Plate 02 - KU4502-C page [56](#)
6. 60° Plate assembly - KU6000-C page [57](#)
7. 60° Plate 01 - KU6001-C page [58](#)
8. 60° Plate 02 - KU6002-C page [59](#)
9. 75° Plate assembly - KU7500-C page [60](#)
10. 75° Plate 01 - KU7501-C page [61](#)
11. 75° Plate 02 - KU7502-C page [62](#)



E	Eenheid : mm	R.	Tekenaar(s) :	Datum :	E	
	ISO 1101 ISO 1302 ISO 2768-mK ISO 8015 ①		1 - 2 - 3 - 4 - 5 - 6 -	- - - - -		
	Schaal : 1:1	lang zwaluwstuk_rol25 11/06/2019 14:59:34				
	Formaat : A4	Tekeninglabel/-nummer :				
F			Odisee Studiegebied IWT Ontwerp- en productietechnologie		-	F



E	Eenheid : mm	R. Tekenaar(s) :	Datum :	E
	ISO 1101 ISO 1302 ISO 2768-mK ISO 8015 ①		1 - 2 - 3 - 4 - 5 - 6 -	
	Schaal : 1:1	matijs_V50_100_35gr_custom 11/06/2019 16:57:33		
	Formaat : A4	Tekeninglabel/-nummer :		
F	 Odisee Studiegebied IWT Ontwerp- en productietechnologie	 Mechanische Ontwerp Productie Technologie	-	F



349.5

A

A

100

45°

01

02

03

04

02

03

04

01

04	KU4501	FOLDED PLATE	1
03	ST0001	M16 C34 Mb DAF BOLT	4
02	ST0002	M16 C34 Mb DAF NUT	4
01	KU4502	FOLDED PLATE	1
P.NO	PART CODE	PART NAME	QTY

Project name OPTIMIZATION OF CASE STUDIES IN HSS BOLTED CONNECTIONS	Created by A.SOLIVERES	Standards ISO 128 ISO 129	Material -	KU4500-C
	Project manager S.COPPIETERS	Technical reference C. JIMENEZ	EN 8015 EN 2768 - c,K DIN 6935	Weight 3.4 kg
	Department MAT. SCIENCE	BOLTED ASSEMBLY		
KU LEUVEN	Scale 1:1	Projection 	Rev C	Date of issue 28/05/2019
	Lang EN	Size A3	Sheet 1/1	

TIGHTENING TORQUE FOR ST0001: 260 Nm + 30°

SECTION A-A

148.9

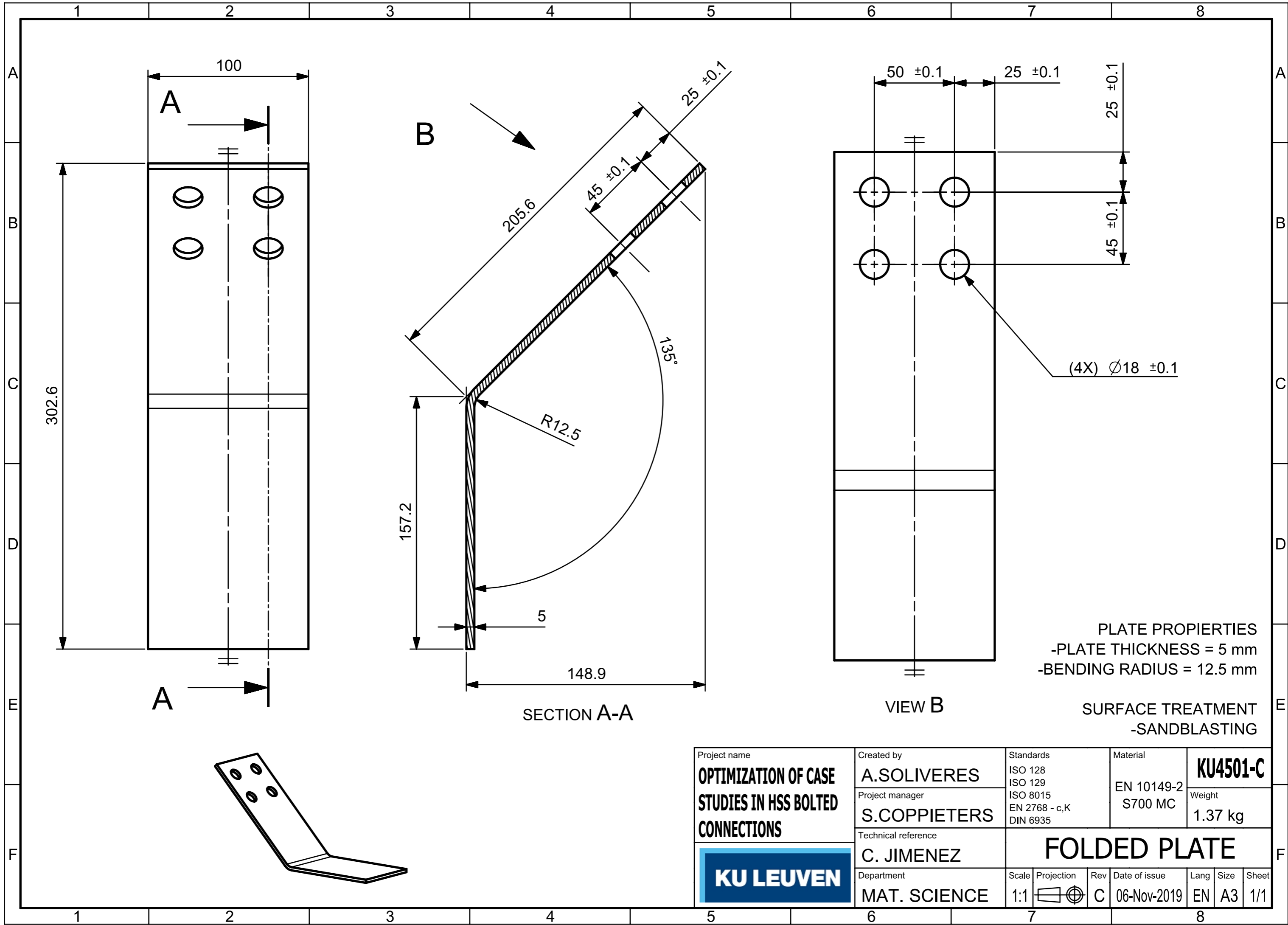


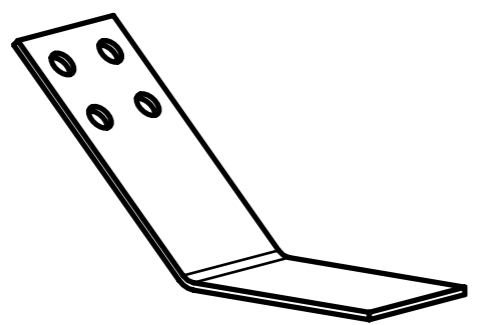
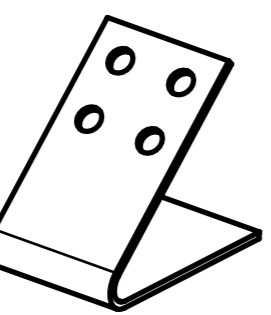
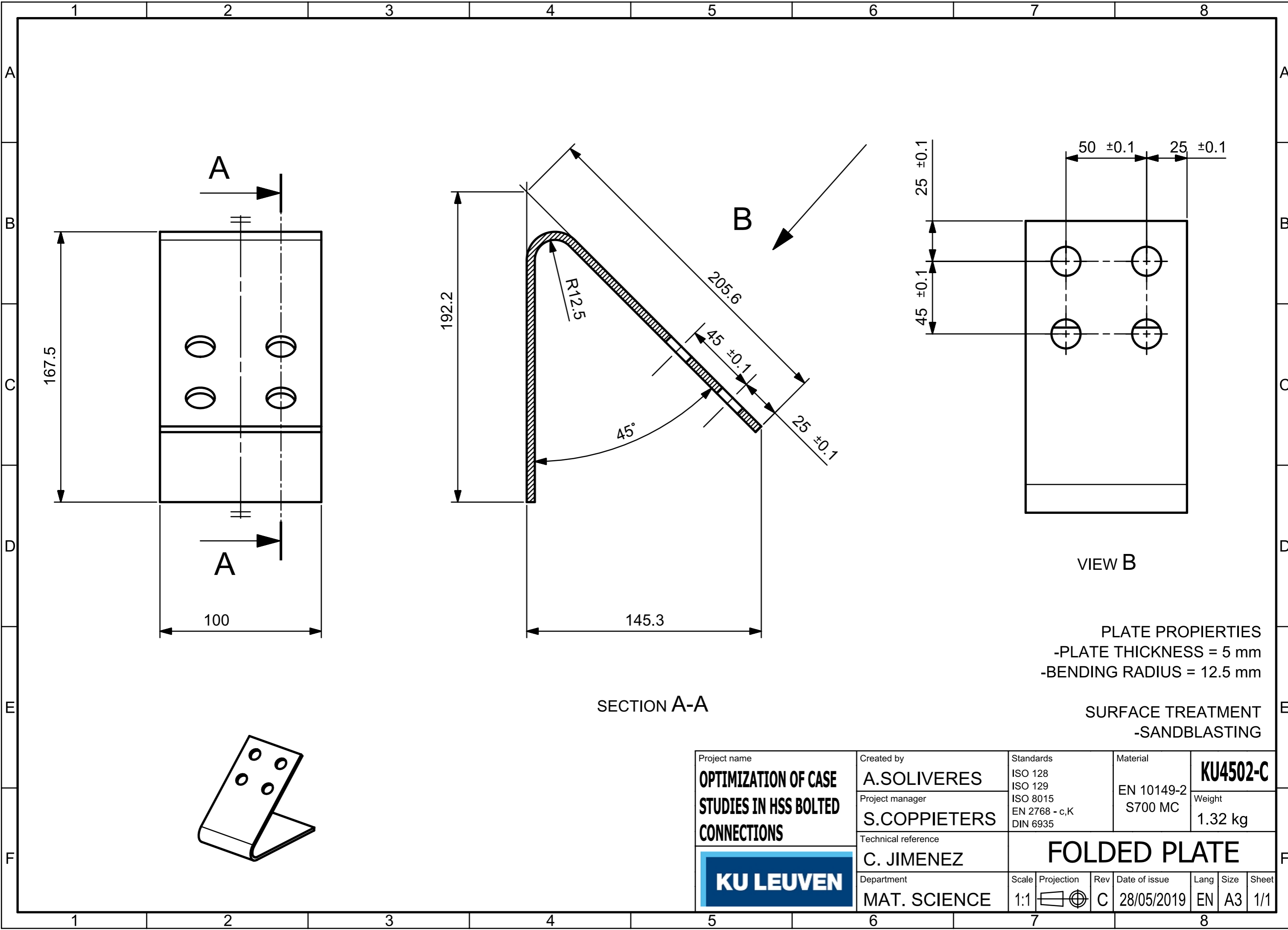


PLATE PROPERTIES
 -PLATE THICKNESS = 5 mm
 -BENDING RADIUS = 12.5 mm
 SURFACE TREATMENT
 -SANDBLASTING

Project name OPTIMIZATION OF CASE STUDIES IN HSS BOLTED CONNECTIONS	Created by A.SOLIVERES	Standards ISO 128 ISO 129 ISO 8015 EN 2768 - c,K DIN 6935	Material EN 10149-2 S700 MC	KU4501-C				
	Project manager S.COPPIETERS	FOLDED PLATE						
	Technical reference C. JIMENEZ	Scale 1:1	Projection 	Rev C	Date of issue 06-Nov-2019	Lang EN	Size A3	Sheet 1/1





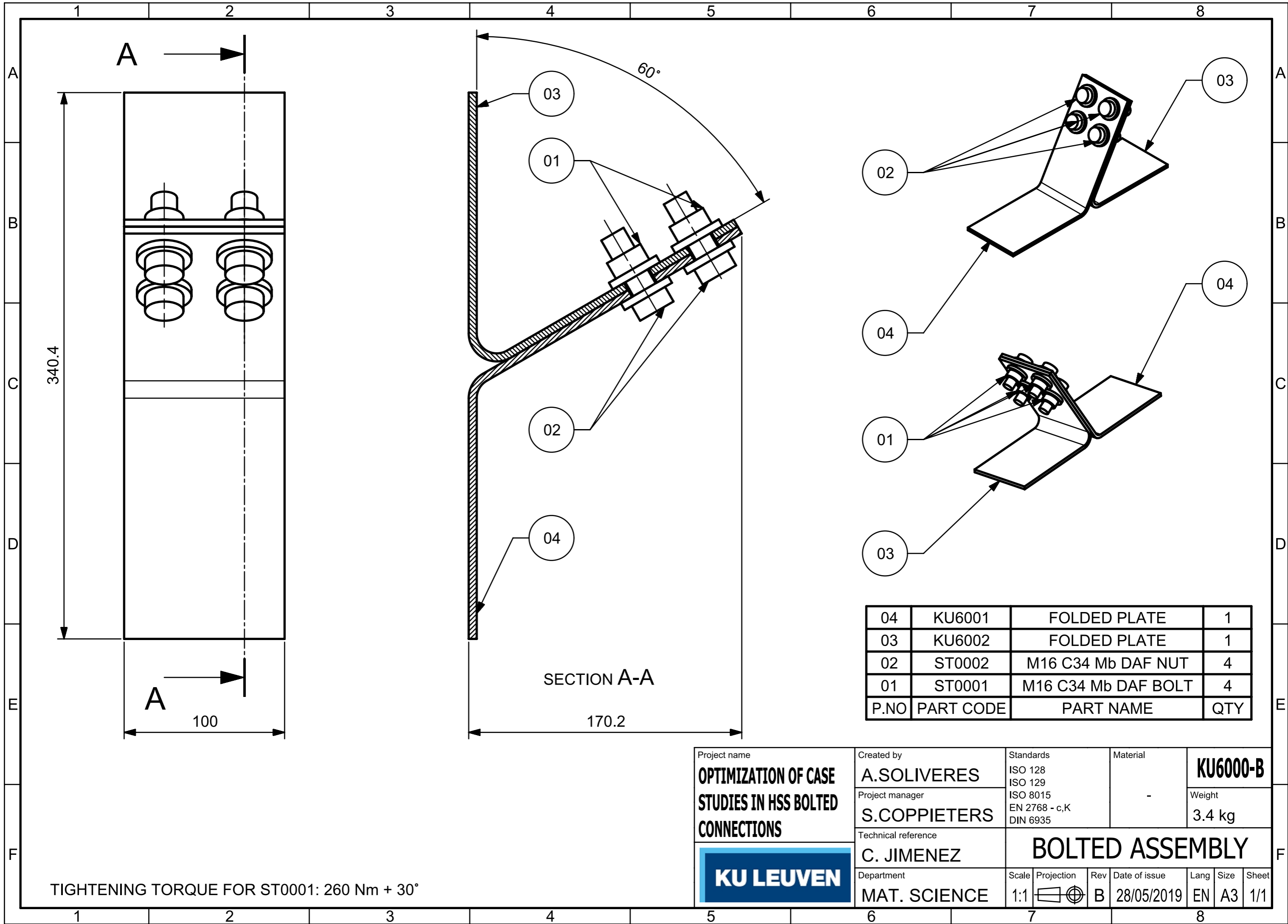
SECTION A-A

VIEW B

PLATE PROPERTIES
 -PLATE THICKNESS = 5 mm
 -BENDING RADIUS = 12.5 mm

SURFACE TREATMENT
 -SANDBLASTING

Project name OPTIMIZATION OF CASE STUDIES IN HSS BOLTED CONNECTIONS	Created by A.SOLIVERES	Standards ISO 128 ISO 129	Material EN 10149-2 S700 MC	KU4502-C
	Project manager S.COPPIETERS	Technical reference C. JIMENEZ	EN 2768 - c,K DIN 6935	Weight 1.32 kg
	Department MAT. SCIENCE	Scale 1:1	Projection 	Rev C
	FOLDED PLATE			
		Lang EN	Size A3	Sheet 1/1

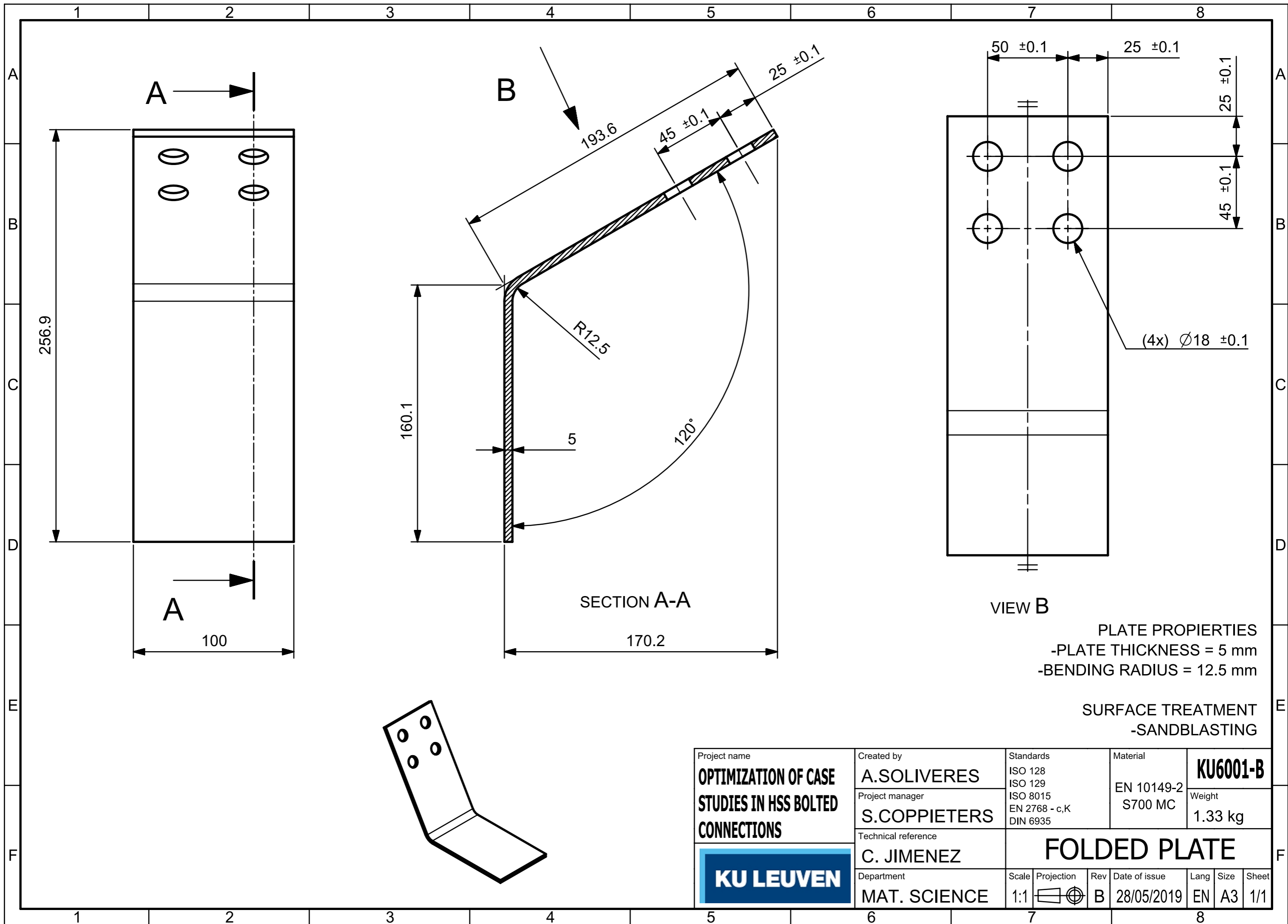


04	KU6001	FOLDED PLATE	1
03	KU6002	FOLDED PLATE	1
02	ST0002	M16 C34 Mb DAF NUT	4
01	ST0001	M16 C34 Mb DAF BOLT	4
P.NO	PART CODE	PART NAME	QTY

Project name OPTIMIZATION OF CASE STUDIES IN HSS BOLTED CONNECTIONS	Created by A.SOLIVERES	Standards ISO 128 ISO 129 ISO 8015 EN 2768 - c,K DIN 6935	Material -	KU6000-B			
	Project manager S.COPPIETERS	Weight 3.4 kg					
	Technical reference C. JIMENEZ	BOLTED ASSEMBLY					
Department MAT. SCIENCE	Scale 1:1	Projection 	Rev B	Date of issue 28/05/2019	Lang EN	Size A3	Sheet 1/1

TIGHTENING TORQUE FOR ST0001: 260 Nm + 30°





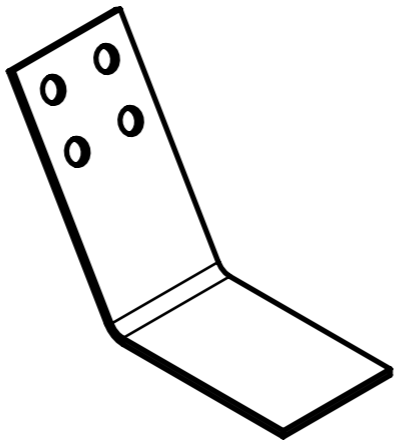
A
B
C
D
E
F

A
B
C
D
E
F

PLATE PROPERTIES
 -PLATE THICKNESS = 5 mm
 -BENDING RADIUS = 12.5 mm

SURFACE TREATMENT
 -SANDBLASTING

Project name OPTIMIZATION OF CASE STUDIES IN HSS BOLTED CONNECTIONS	Created by A.SOLIVERES	Standards ISO 128 ISO 129 ISO 8015 EN 2768 - c,K DIN 6935	Material EN 10149-2 S700 MC	KU6001-B
	Project manager S.COPPIETERS	Weight 1.33 kg		
	Technical reference C. JIMENEZ	FOLDED PLATE		
Department MAT. SCIENCE	Scale 1:1	Projection 	Rev B	Date of issue 28/05/2019
		Lang EN	Size A3	Sheet 1/1



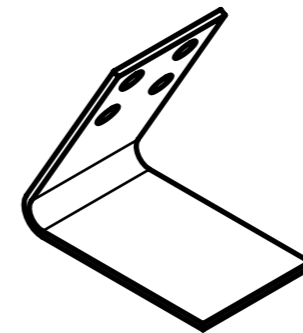
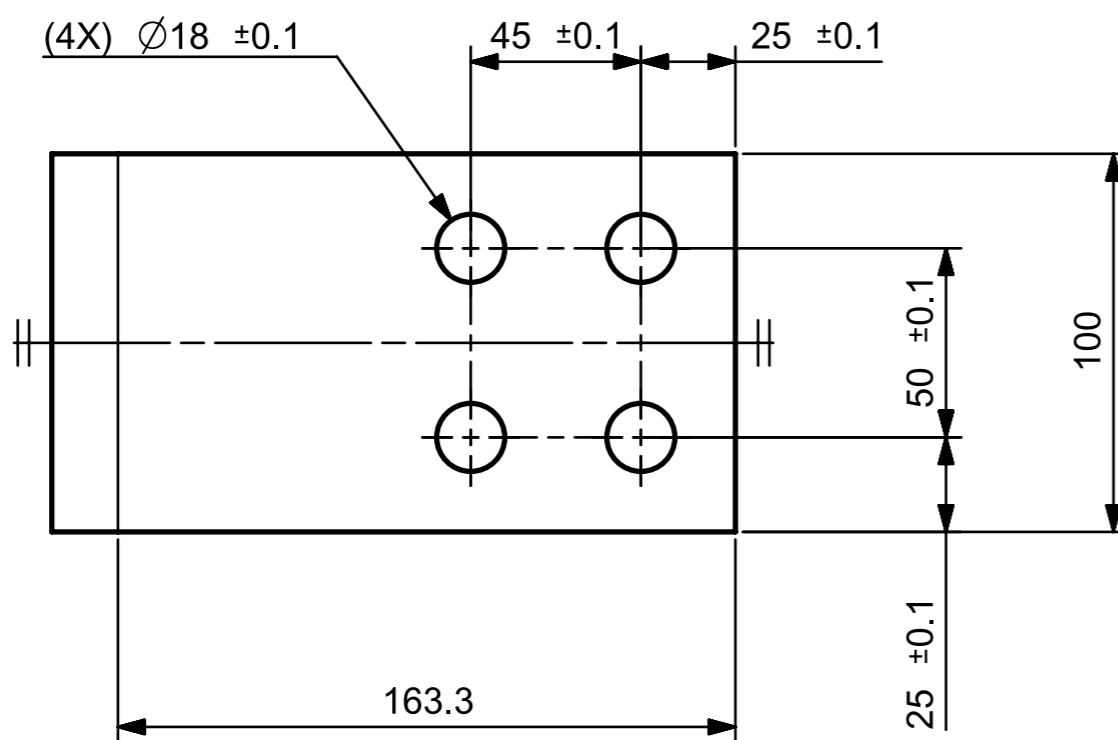
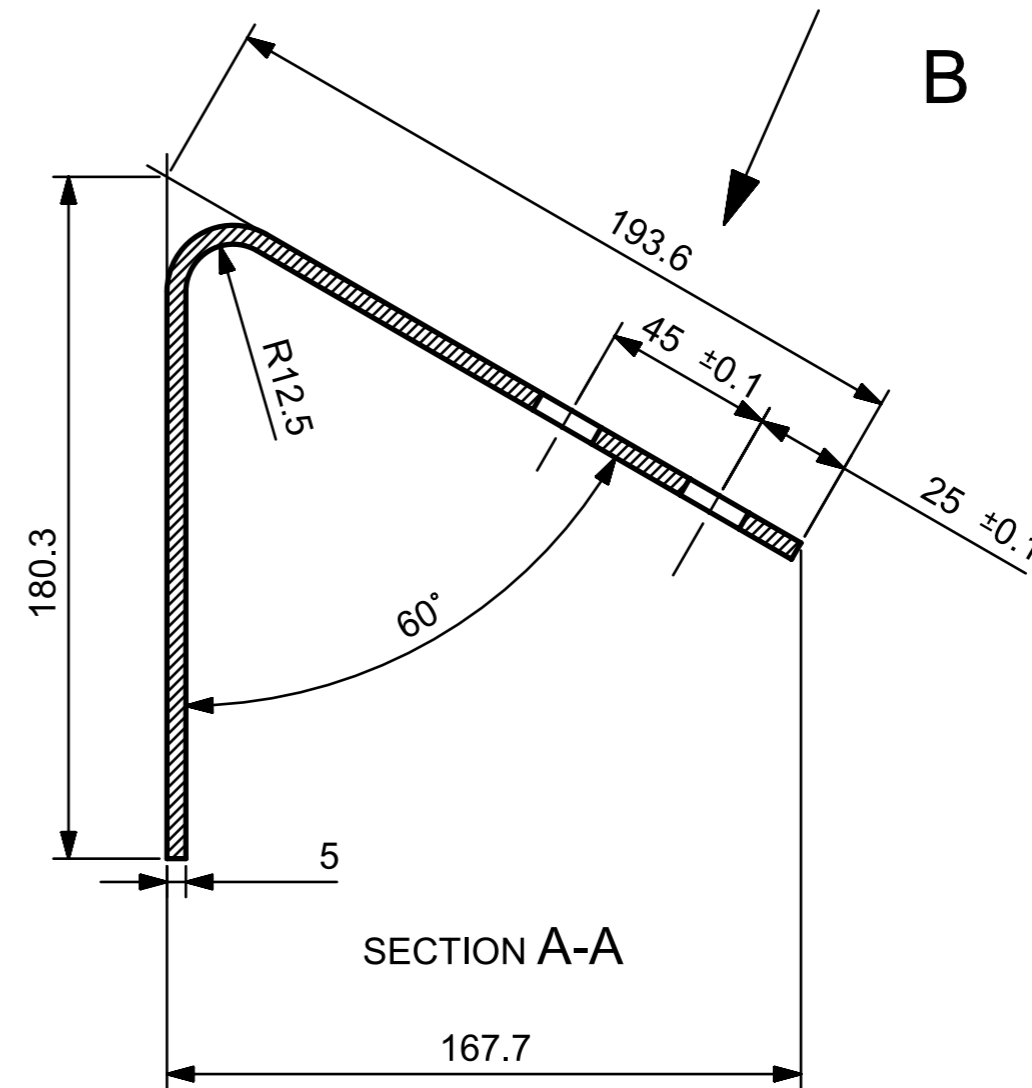
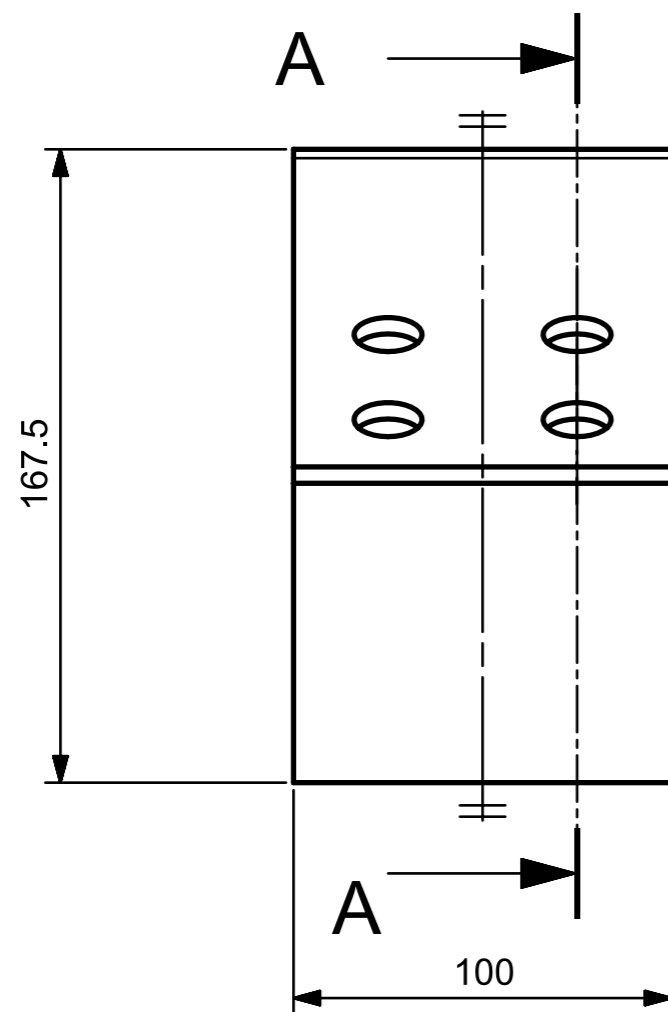


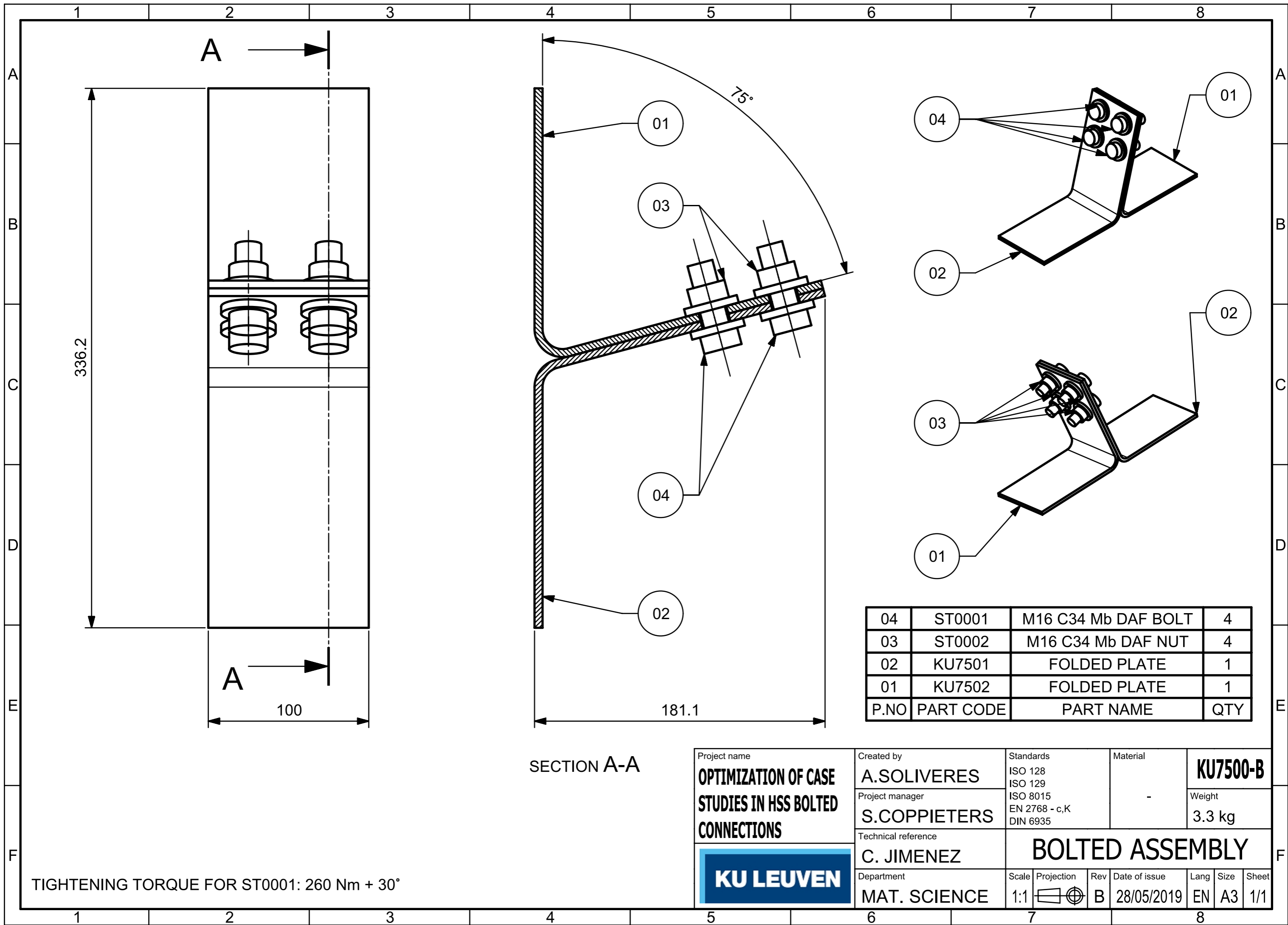
PLATE PROPERTIES
 -PLATE THICKNESS = 5 mm
 -BENDING RADIUS = 12.5 mm

SURFACE TREATMENT
 -SANDBLASTING

Project name OPTIMIZATION OF CASE STUDIES IN HSS BOLTED CONNECTIONS	Created by A.SOLIVERES	Standards ISO 128 ISO 129 ISO 8015 EN 2768 - c,K DIN 6935	Material EN 10149-2 S700 MC	KU6002-B			
	Project manager S.COPPIETERS	Weight 1.33 kg					
	Technical reference C. JIMENEZ	FOLDED PLATE					
Department MAT. SCIENCE	Scale 1:1	Projection 	Rev B	Date of issue 28/05/2019	Lang EN	Size A3	Sheet 1/1



VIEW B



336.2

A →

A →



100

75°

181.1

SECTION A-A

04	ST0001	M16 C34 Mb DAF BOLT	4
03	ST0002	M16 C34 Mb DAF NUT	4
02	KU7501	FOLDED PLATE	1
01	KU7502	FOLDED PLATE	1
P.NO	PART CODE	PART NAME	QTY

Project name OPTIMIZATION OF CASE STUDIES IN HSS BOLTED CONNECTIONS	Created by A.SOLIVERES	Standards ISO 128 ISO 129	Material -	KU7500-B				
	Project manager S.COPPIETERS	Technical reference C. JIMENEZ	EN 2768 - c,K DIN 6935	Weight 3.3 kg				
	Department MAT. SCIENCE	BOLTED ASSEMBLY						
		Scale 1:1	Projection 	Rev B	Date of issue 28/05/2019	Lang EN	Size A3	Sheet 1/1

TIGHTENING TORQUE FOR ST0001: 260 Nm + 30°

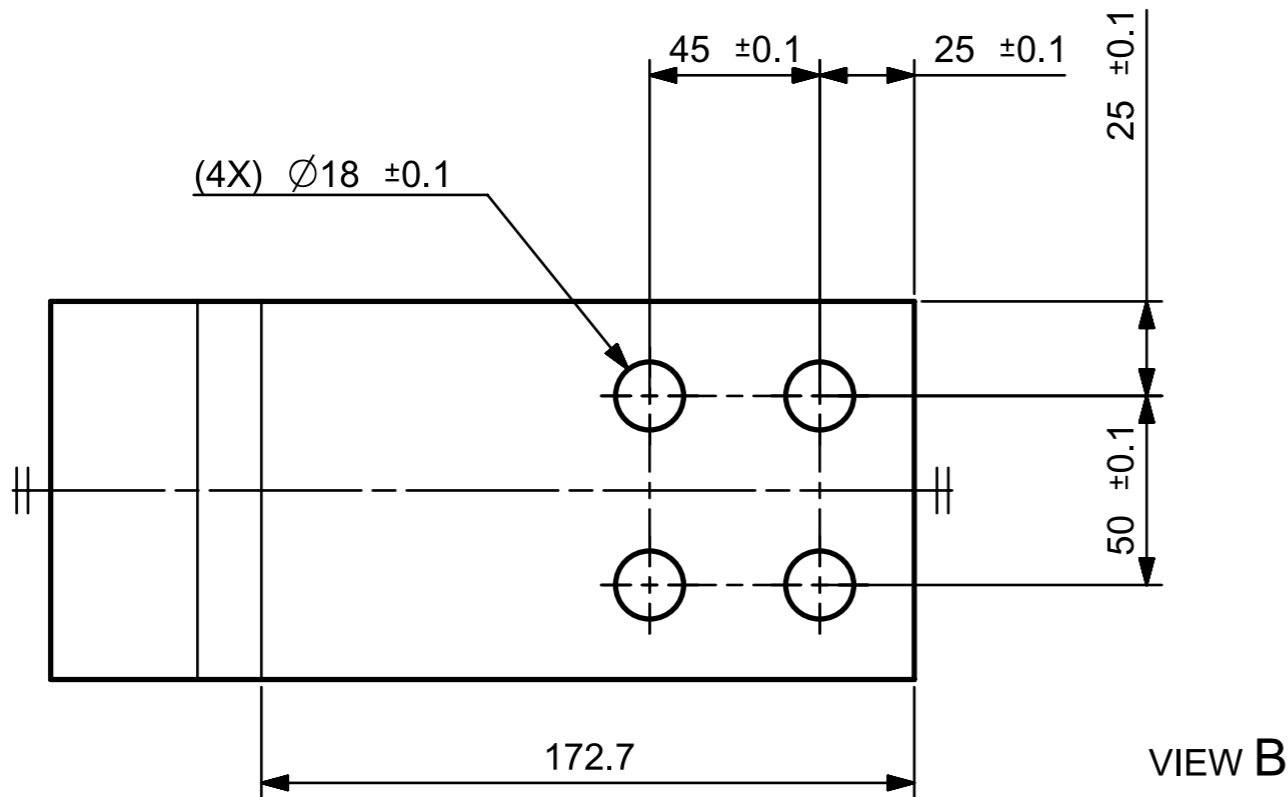
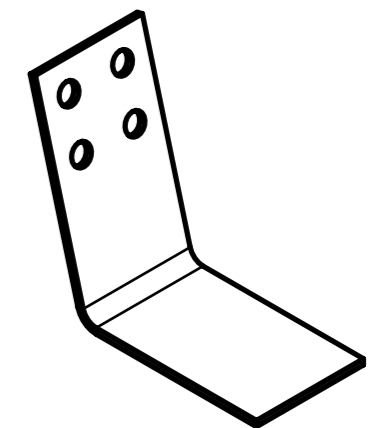
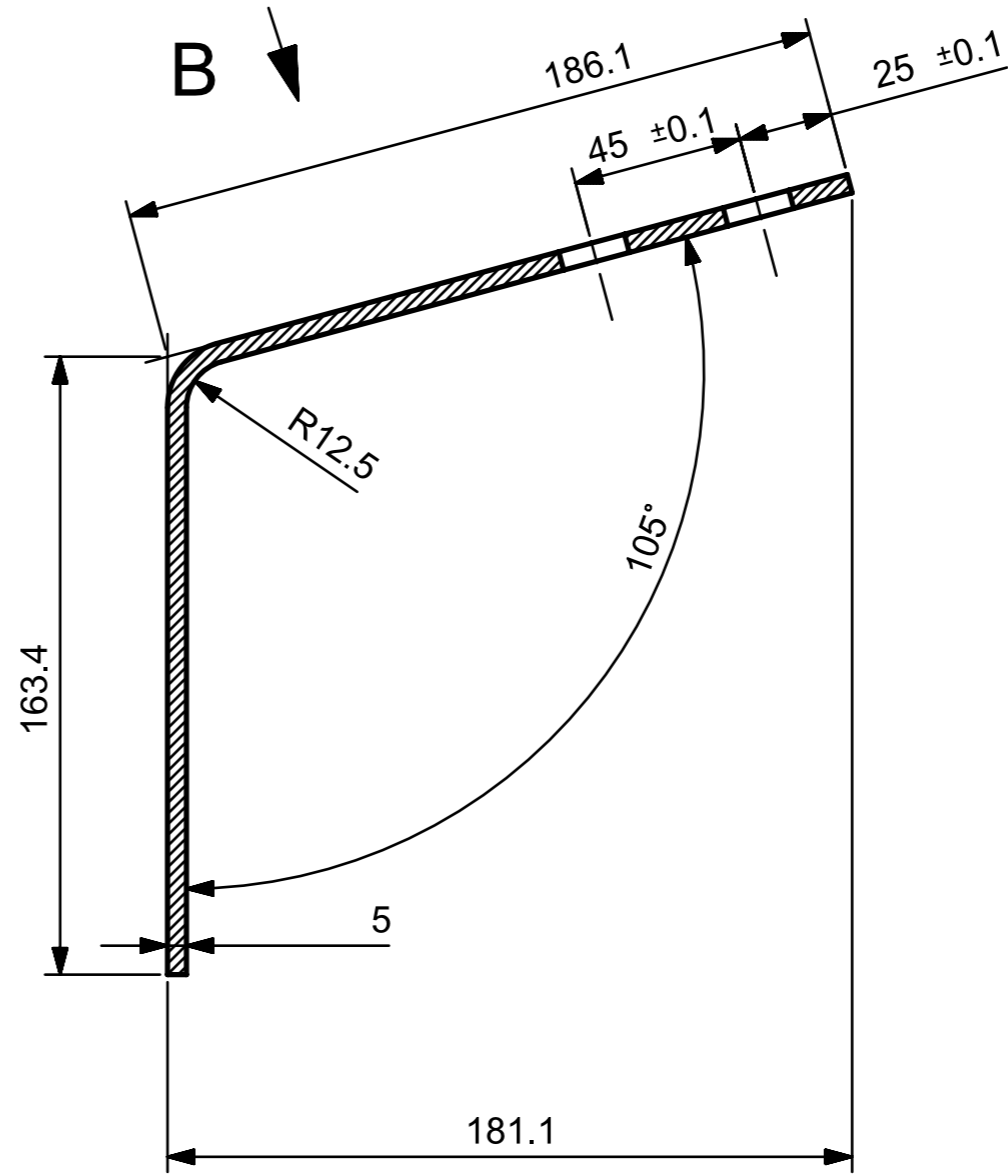
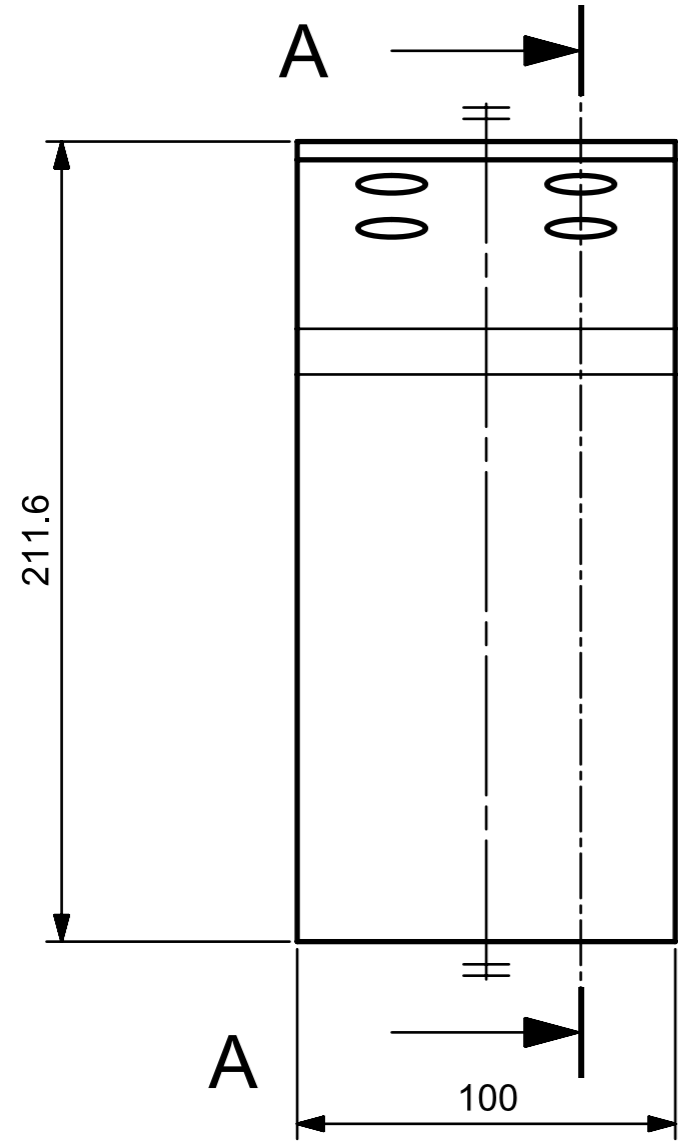


PLATE PROPERTIES
 -PLATE THICKNESS = 5 mm
 -BENDING RADIUS = 12.5 mm

SURFACE TREATMENT
 -SANDBLASTING

Project name OPTIMIZATION OF CASE STUDIES IN HSS BOLTED CONNECTIONS	Created by A.SOLIVERES	Standards ISO 128 ISO 129 ISO 8015 EN 2768 - c,K DIN 6935	Material EN 10149-2 S700 MC	KU7501-B			
	Project manager S.COPPIETERS	Weight 1.30 kg					
	Technical reference C. JIMENEZ	FOLDED PLATE					
Department MAT. SCIENCE	Scale 1:1	Projection 	Rev B	Date of issue 28/05/2019	Lang EN	Size A3	Sheet 1/1



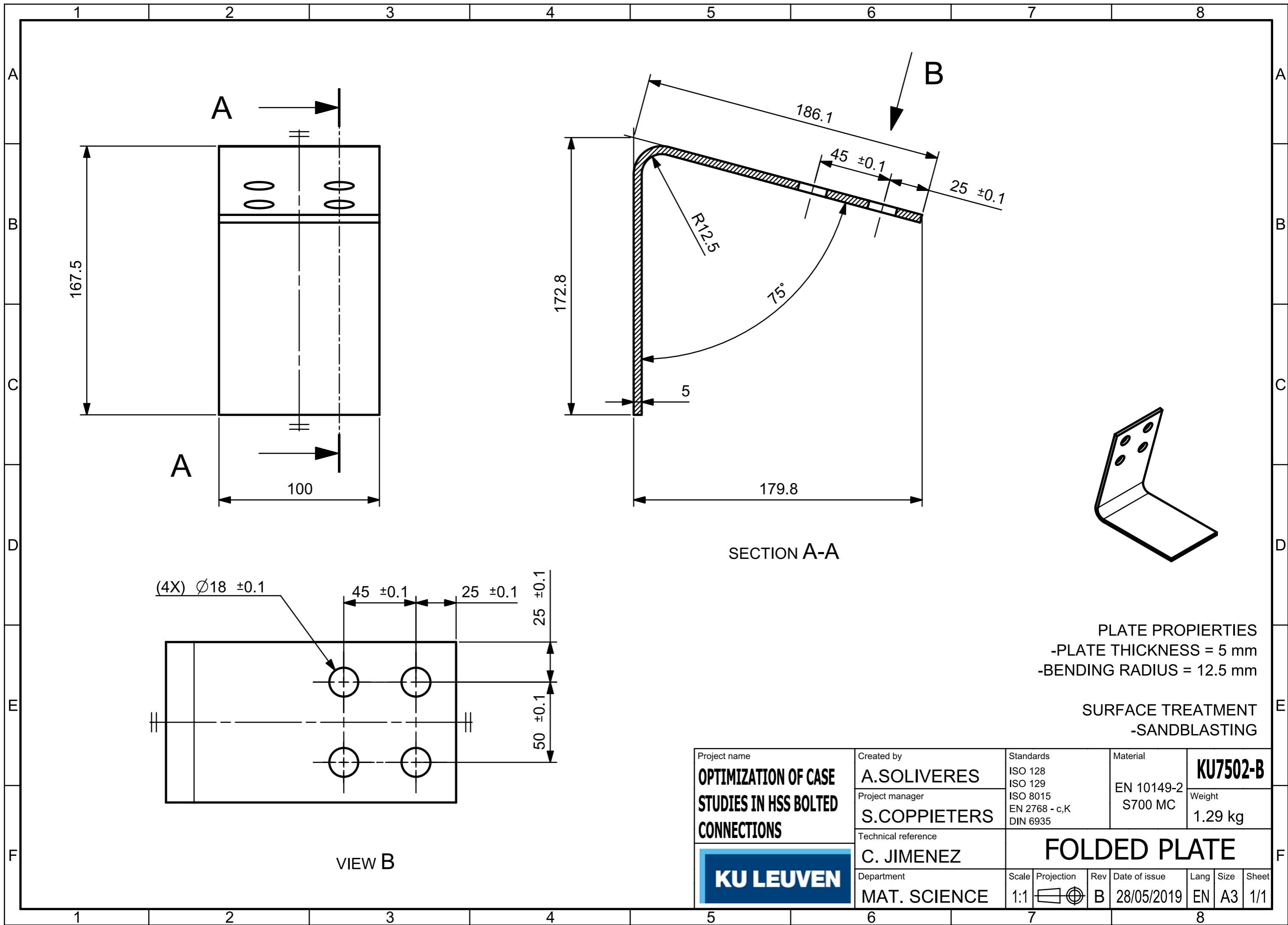


PLATE PROPERTIES
 -PLATE THICKNESS = 5 mm
 -BENDING RADIUS = 12.5 mm

SURFACE TREATMENT
 -SANDBLASTING

Project name OPTIMIZATION OF CASE STUDIES IN HSS BOLTED CONNECTIONS	Created by A.SOLIVERES	Standards ISO 128 ISO 129 ISO 8015 EN 2768 - c,K DIN 6935	Material EN 10149-2 S700 MC	KU7502-B			
	Project manager S.COPPIETERS	Weight 1.29 kg					
	Technical reference C. JIMENEZ	FOLDED PLATE					
Department MAT. SCIENCE	Scale 1:1	Projection 	Rev B	Date of issue 28/05/2019	Lang EN	Size A3	Sheet 1/1



Appendix B

Design parametrization and scripting

When a design procedure starts a wide range of parameters have to be taking in account in order to reach a final configuration. Since a wide range of variations are mean to be introduced in the specimen design in the first stages of the model definition a parametric approach is determined.

This approach enables the designer to modify a a vast number of parameters without editing each 3D operation or making any assembly adjustments. The parametric 3D design approach used in the project assemblies definition is explained in this appendix.

B.1 Design parametrization

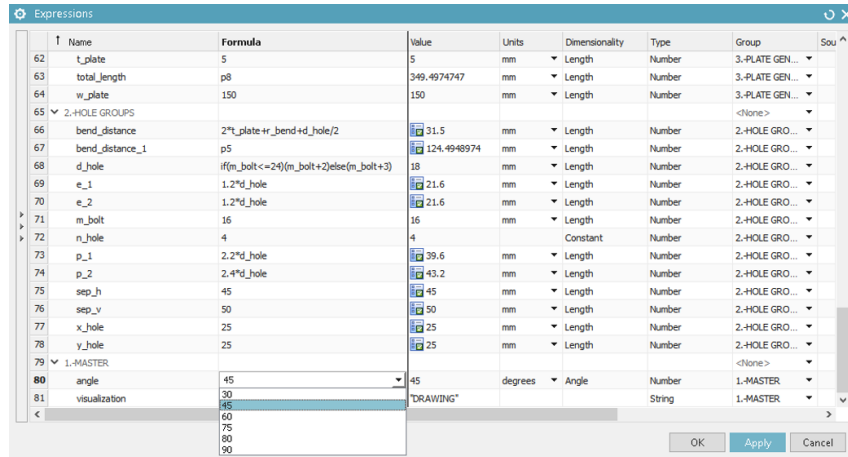
Firstly the design variables are parametrised using the NX Unigraphics software. To do so the NX expressions module within the modelling app is used, this module is capable of controlling the relations between the features of a component and the components determination inside of an assembly by varying the expressions values listed in the system.

A combination model assembly expressions and inter-part expressions are used in the design of the assembly. This elements allow design changes in the main assembly as well as in any part component by editing the expressions value without bothering changing every design feature or sketch editing.

At the beginning the parametrisation makes the design process slower and can be seen as a very time consuming activity when the design is in its first steps but since numerous design iterations are needed to reach the final model the parametrization capability gives us the option of analyse the model variations in each of the pieces by changing values in the main assembly.

This is very convenient not only to determine the influence of the design parameters but also to create a range of elements as in our case with the angle modifications so the assembly has to be defined only once and the rest of the assembly dispositions are generated by modifying the parameters.

B. DESIGN PARAMETRIZATION AND SCRIPTING



#	Name	Formula	Value	Units	Dimensionality	Type	Group
62	t_plate	5	5	mm	Length	Number	3-PLATE GEN...
63	total_length	p8	349.4974747	mm	Length	Number	3-PLATE GEN...
64	w_plate	150	150	mm	Length	Number	3-PLATE GEN...
65	2-HOLE GROUPS						
66	bend_distance	2*t_plate+r_bend+d_hole/2	31.5	mm	Length	Number	2-HOLE GRO...
67	bend_distance_1	p5	124.4948974	mm	Length	Number	2-HOLE GRO...
68	d_hole	if(m_bolt <= 24)(m_bolt+2)else(m_bolt+3)	18	mm	Length	Number	2-HOLE GRO...
69	e_1	1.2*d_hole	21.6	mm	Length	Number	2-HOLE GRO...
70	e_2	1.2*d_hole	21.6	mm	Length	Number	2-HOLE GRO...
71	m_bolt	16	16	mm	Length	Number	2-HOLE GRO...
72	n_hole	4	4		Constant	Number	2-HOLE GRO...
73	p_1	2.2*d_hole	39.6	mm	Length	Number	2-HOLE GRO...
74	p_2	2.4*d_hole	43.2	mm	Length	Number	2-HOLE GRO...
75	sep_h	45	45	mm	Length	Number	2-HOLE GRO...
76	sep_v	50	50	mm	Length	Number	2-HOLE GRO...
77	x_hole	25	25	mm	Length	Number	2-HOLE GRO...
78	y_hole	25	25	mm	Length	Number	2-HOLE GRO...
79	1-MASTER						
80	angle	45	45	degrees	Angle	Number	1-MASTER
81	visualization	"DRAWING"				String	1-MASTER

Figure B.1: NX expressions module

Thanks to this parametrised features several parameters are tested too so the agreement radius influence, the angle and overall length values are analysed without the need of defining a whole model from scratch or to delve into the operations of each model to change the desired values.

For each design modification in the parameters an assembly is exported in .spt format from NX to be analysed in Abaqus. But before the assembly is exported and in order to save computational time another parameter is introduced in the assembly. This one creates a half cut in each of the plates and suppress the bolt and nuts in the cut part. Also the clamping distance is removed from the plates.

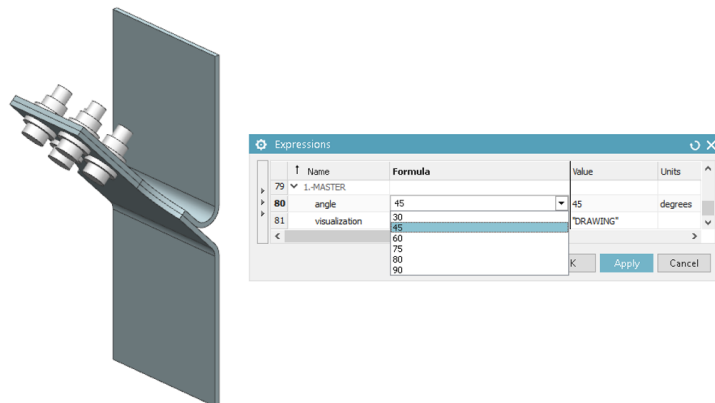
This assembly simplification can be seen in [Fig. B.3](#) and saves us a lot of computational times since the behaviour for each part of the assembly is symmetrical. The clamping area is also removed to save computational time by reducing the mesh elements number in each of the plate.

B.2 Abaqus scripting

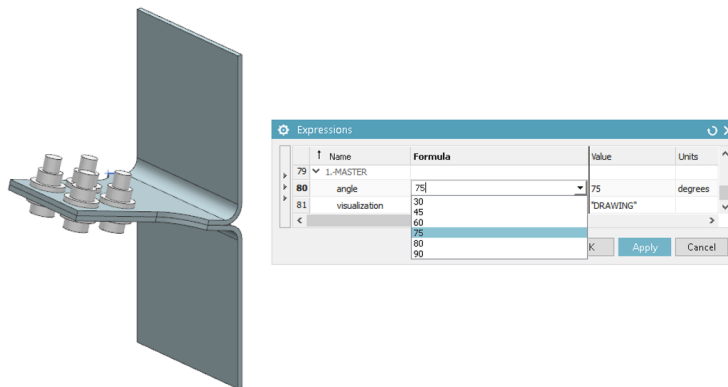
Due to the high amount of design variations to test for each model variation an Abaqus script has been developed. This script is capable of generating the Abaqus analysis job for all the plate variation parameters disposed in this test.

Using the Python language integration with Abaqus an script to define the testing model parameters can be defined. In this script the .spt file of the model is imported, and it retrieves us the .inp file ready to send it to the server in order to get the calculations.

This scripts are a real time saver since them generate the materials, interactions partitions and mesh for every model modification in the model just by changing the model name in the script. The Abaqus documentation [\[57\]](#), [\[58\]](#) has probed to be crucial to correctly develop the scripts since it prevents the programmer from the trial and error iterations that can be very time consuming .



(a) Parameter modification: Plate 1 \angle 45°



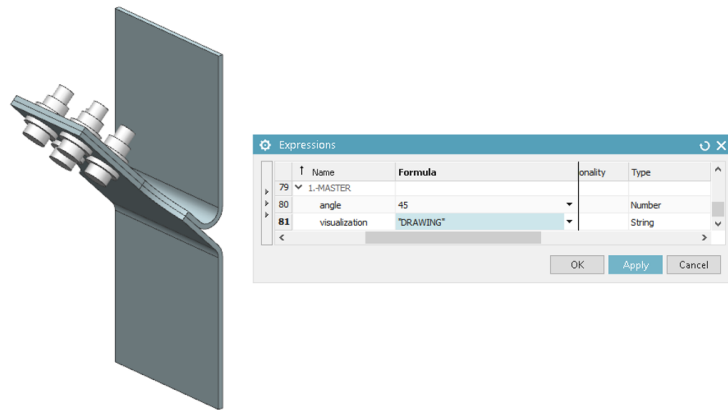
(b) Parameter modification: Plate 1 \angle 75°

Figure B.2: Angle parameter modifications

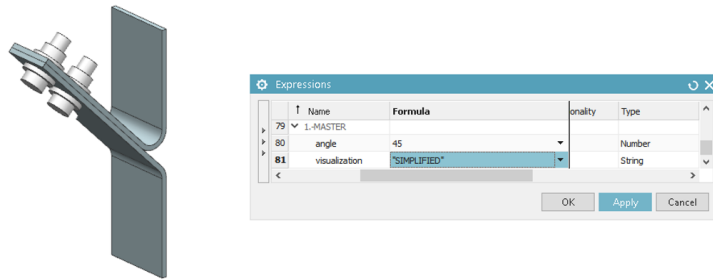
The Abaqus scripting feature has not been only used to define the analysis parameters but is also used to obtain data from the .ODB file. Since it is really useful to analyse the numerical data in a graphic way the script is defined in a way that retrieves stress, strain, shear stress and contact slip around a tangential path in the contact zone and returns a the plots with the selected data and a .CSV file with all the numerical ready to be plotted and compared in excel.

The whole scripting integration process is depicted in [Fig. B.4](#)

B. DESIGN PARAMETRIZATION AND SCRIPTING



(a) Model definition for the drawings and production



(b) Simplified model definition for numerical analysis

Figure B.3: Model representations

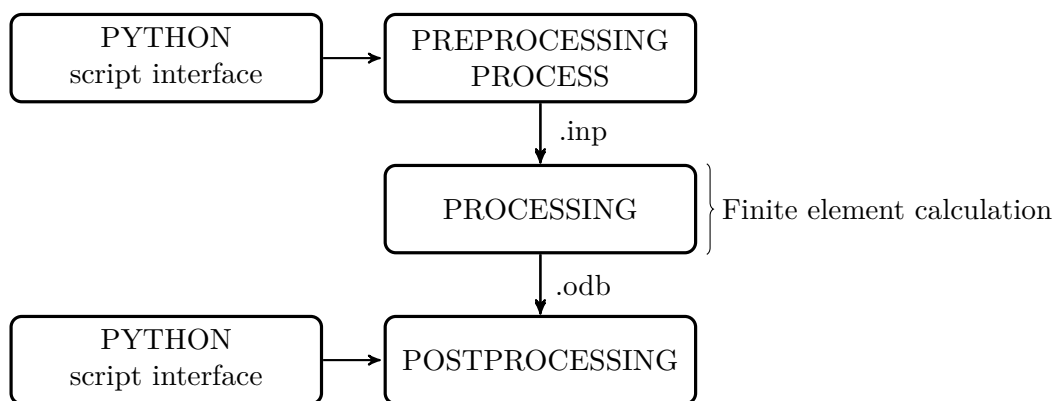


Figure B.4: Abaqus python Scripting integration flow diagram

Bibliography

- [1] *EN 1993-1-12. Eurocode 3: design of steel structures - Part 1-12: additional rules for the extension of EN 1993 up to steel grades S 700. Brussels: European Committee for Standardisation; 2007.* 1994.
- [2] *European structural steel standard EN 10025-2 : 2004.* 2004.
- [3] *Eurocode 3: Design of steel structures - Part 1-8: Design of joints. Brussels: European Committee for Standardisation; 2007.* 2005.
- [4] E. T. Akinlabi, S. A. Akinlabi, and E. Ogunmuyiwa. Characterising the effects of sand blasting on formed steel samples. 2013.
- [5] A. Benhamena, A. Talha, N. Benseddiq, A. Amrouche, G. Mesmacque, and M. Benguediab. Effect of clamping force on fretting fatigue behaviour of bolted assemblies: Case of couple steel–aluminium. *Materials Science and Engineering: A*, 527(23):6413–6421, 2010.
- [6] A. A. Bhatti, Z. Barsoum, V. Van Der Mee, A. Kromm, and T. Kannengießer. Fatigue strength improvement of welded structures using new low transformation temperature filler materials. *Procedia Engineering*, 66:192–201, 2013.
- [7] E. Brezova, H. Masiar, and P. Radic. Welding of high strength materials used in the manufacture special equipment. *University review*, 8(3-4):51–61, 2014.
- [8] K. H. Brown, C. W. Morrow, S. Durbin, and A. Baca. Guideline for bolted joint design and analysis: version 1.0. Technical report, Sandia National Laboratories, 2008.
- [9] T. Chakherlou, M. Razavi, A. Aghdam, and B. Abazadeh. An experimental investigation of the bolt clamping force and friction effect on the fatigue behavior of aluminum alloy 2024-t3 double shear lap joint. *Materials & Design*, 32(8-9):4641–4649, 2011.
- [10] X. Chen, S. Xu, and D. Huang. A critical plane-strain energy density criterion for multiaxial low-cycle fatigue life under non-proportional loading. *Fatigue & Fracture of Engineering Materials & Structures*, 22(8):679–686, 1999.
- [11] P. R. Childs. *Mechanical design engineering handbook*. Butterworth-Heinemann, 2013.

- [12] P. Collin and B. Johansson. Eurocode for high strength steel and applications in construction. In *International Conference Super-High Strength Steels: 02/11/2005-04/11/2005*. Associazione Italiana di Metallurgia, 2005.
- [13] O. Corp. Omax 55100 jetmachining center. URL: https://www.omax.com/sites/default/files/media/specsheets/600038d_-_55100.pdf, last checked on 2019-06-21.
- [14] CORROSIONPEDIA. Sand blasting. URL: <https://www.corrosionpedia.com/definition/1003/sand-blasting>, last checked on 2019-06-23.
- [15] Hot rolled flat products made of high yield strength steels for cold forming - Part 2: Technical delivery conditions for thermomechanically rolled steels. Standard, DIN, Dec. 2013.
- [16] S. F. Enterprises. Sunnforest garnet for waterjet cutting. URL: <https://www.sunnforest.com/Industrial-Minerals/Garnet/Garnet-for-Blasting.html>, last checked on 2019-06-24.
- [17] EUR-Lex. Road safety: authorised dimensions and maximum weights for trucks, buses and coaches. URL: <https://eur-lex.europa.eu/legal-content/EN/TXT/PDF/?uri=CELEX:31996L0053&from=EN>, last checked on 2019-05-23.
- [18] A. Fatemi and D. F. Socie. A critical plane approach to multiaxial fatigue damage including out-of-phase loading. *Fatigue & Fracture of Engineering Materials & Structures*, 11(3):149–165, 1988.
- [19] L. Group. Ppeb series. URL: https://www.lvdgroup.com/sites/default/files/downloads/ppeb_us_0.pdf, last checked on 2019-06-21.
- [20] O.-P. Hämmäläinen and T. Björk. Fretting fatigue phenomenon in bolted high-strength steel plate connections. *Steel Construction*, 8(3):174–178, 2015.
- [21] S. Heimbs, S. Schmeer, J. Blaurock, and S. Steeger. Static and dynamic failure behaviour of bolted joints in carbon fibre composites. *Composites Part A: Applied Science and Manufacturing*, 47:91–101, 2013.
- [22] R. Hojjati Talemi, M. Abdel Wahab, T. Yue, and L. D’Alvise. On fretting fatigue behaviour of single bolted lap joint. In *3rd International Journal of Fracture Fatigue and Wear*, volume 2, pages 269–274. Laboratory Soete–Ghent University, 2014.
- [23] J. Hu, Z. Marciniak, and J. Duncan. *Mechanics of sheet metal forming*. Elsevier, 2002.
- [24] Welding and allied processes - Symbolic representation on drawings - Welded joints. Standard, ISO, Mar. 2019.
- [25] Welding and allied processes – Nomenclature of processes and reference numbers. Standard, ISO, Aug. 2009.

-
- [26] U. L. Z. V. JEKLA. Fatigue properties of a high-strength-steel welded joint. *Materiali in tehnologije*, 41(4):163–166, 2007.
- [27] Y. Jiang, O. Hertel, and M. Vormwald. An experimental evaluation of three critical plane multiaxial fatigue criteria. *International Journal of Fatigue*, 29(8):1490–1502, 2007.
- [28] C. Jiménez-Peña, R. H. Talemi, B. Rossi, and D. Debruyne. Investigations on the fretting fatigue failure mechanism of bolted joints in high strength steel subjected to different levels of pre-tension. *Tribology International*, 108:128–140, 2017.
- [29] P. Kah, M. Pirinen, R. Suoranta, and J. Martikainen. Welding of ultra high strength steels. In *Materials Engineering and Technology*, volume 849 of *Advanced Materials Research*, pages 357–365. Trans Tech Publications Ltd, 2014.
- [30] M. Khan. *Welding Science and Technology*. New Age International (P) Limited, 2007.
- [31] H. S. Kim and S. Mall. Investigation into three-dimensional effects of finite contact width on fretting fatigue. *Finite elements in analysis and design*, 41(11-12):1140–1159, 2005.
- [32] J. Kim, J.-C. Yoon, and B.-S. Kang. Finite element analysis and modeling of structure with bolted joints. *Applied mathematical modelling*, 31(5):895–911, 2007.
- [33] C. Knight. *A Finite Element Method Primer for Mechanical Design*. PWS series in engineering. PWS Pub., 1994.
- [34] D. Krajcarz. Comparison metal water jet cutting with laser and plasma cutting. *Procedia Engineering*, 69:838–843, 2014.
- [35] Y. Ling, H. Lee, and B. Cheok. Finite element analysis of springback in l-bending of sheet metal. *Journal of Materials Processing Technology*, 168(2):296–302, 2005.
- [36] J. Liu. Eakest link theory and multiaxial criteria. In *European Structural Integrity Society*, volume 25, pages 55–68. Elsevier, 1999.
- [37] S. Lo and C. Lee. On using meshes of mixed element types in adaptive finite element analysis. *Finite Elements in Analysis and Design*, 11(4):307–336, 1992.
- [38] J. Madge, S. Leen, and P. Shipway. A combined wear and crack nucleation–propagation methodology for fretting fatigue prediction. *International Journal of Fatigue*, 30(9):1509–1528, 2008.
- [39] MatchID. Metrology beyond colors. URL: <https://www.matchid.eu>, last checked on 2019-06-24.

- [40] T. Mert. Water jet cutting technology and its comparison with other cutting methods in some aspects. 2012.
- [41] A. Mittal. A22 - amstrong ultra - ultra high strength steels. URL: https://industry.arcelormittal.com/catalogue/A22/EN#grade_2918, last checked on 2019-05-23.
- [42] M. Mohammadpour, M. Kalajahi, R. Oskouei, and M. Shakouri. Fatigue life estimation of coach peel riveted joints using multi-axial fatigue criteria. *Materials & Design (1980-2015)*, 62:327–333, 2014.
- [43] H.-S. Nah, H.-J. Lee, K.-S. Kim, J.-H. Kim, and W.-B. Kim. Evaluating relaxation of high-strength bolts by parameters on slip faying surfaces of bolted connections. *International Journal of Steel Structures*, 10(3):295–303, 2010.
- [44] NANOSTEEL. Targeted ahss properties. URL: <https://nanosteelco.com/products/sheet-steel/targeted-properties/>, last checked on 2019-05-23.
- [45] R. Norton. *Diseño de máquinas: un enfoque integrado*. Pearson Educación de México, SA de CV, 2011.
- [46] S. I. N.V./S.A. Venti-compact. URL: <https://straaltechniek.net/equipment/blast-cabinets/>, last checked on 2019-06-23.
- [47] U. D. of Energy. 2010 class 8 truck tractor weight by component. URL: <https://www.energy.gov/eere/vehicles/fact-620-april-26-2010-class-8-truck-tractor-weight-component>, last checked on 2019-06-24.
- [48] S. Panthi, N. Ramakrishnan, K. Pathak, and J. Chouhan. An analysis of springback in sheet metal bending using finite element method (fem). *Journal of Materials Processing Technology*, 186(1-3):120–124, 2007.
- [49] Z. D. Perović. Investigation of the fatigue strength of the welded joints treated by tig dressing. *Archives of Materials Science*, 28(1-4):113, 2007.
- [50] K. L. M. O. M. PRODUCTS and PROCESSES. Digital image correlation. URL: <https://iiw.kuleuven.be/onderzoek/mem2p/research/dic>, last checked on 2019-05-22.
- [51] M. Seddeik and J. Kennedy. Deformations in hollow structural section (hss) members subjected to cold-bending. *International journal of mechanical sciences*, 29(3):195–212, 1987.
- [52] R. S. Shoberg. Engineering fundamentals of threaded fastener design and analysis. i. *Fastening*, 6(2):26–29, 2000.
- [53] R. Smith, P. Watson, and T. Topper. A stress-strain parameter for the fatigue of metals. *Journal of Materials*, 5(4):767–778, 1970.

- [54] W. Smith and J. Hashemi. *Foundations of Materials Science and Engineering*. McGraw-Hill Series in Materials Science and Engineering. McGraw-Hill, 2004.
- [55] W. A. Steel. Advanced high-strength steels application guidelines version 6.0. URL: <https://www.worldautosteel.org/projects/advanced-high-strength-steel-application-guidelines/>, last checked on 2019-06-24.
- [56] W. S. Sum, E. J. Williams, and S. B. Leen. Finite element, critical-plane, fatigue life prediction of simple and complex contact configurations. *International Journal of Fatigue*, 27(4):403–416, 2005.
- [57] D. Systemes-SIMULIA. Abaqus scripting user’s guide. URL: <https://www.sharcnet.ca/Software/Abaqus/6.14.2/v6.14/books/cmd/default.htm>, last checked on 2019-05-22.
- [58] D. Systemes-SIMULIA. Abaqus scripting user’s guide. URL: <https://www.sharcnet.ca/Software/Abaqus/6.14.2/v6.14/books/ker/default.htm>, last checked on 2019-05-22.
- [59] M. P. Szolwinski and T. N. Farris. Observation, analysis and prediction of fretting fatigue in 2024-t351 aluminum alloy. *Wear*, 221(1):24–36, 1998.
- [60] S. Thohura and M. S. Islam. Study of the effect of finite element mesh quality on stress concentration factor of plates with holes. *Proceedings of the 15th Annual Paper Meet*, 7(08):19, 2014.
- [61] R. J. Tyrrell. Getting bodies into contact - the despair and joy. URL: https://advancedanalysis.co.uk/AAL/Web_Files/docs/AAL-Getting%20Bodies%20into%20Contact%20-%20the%20Despair%20and%20Joy.pdf, last checked on 2019-06-24.
- [62] R. J. Tyrrell. Getting bodies into contact - the despair and joy. URL: https://advancedanalysis.co.uk/AAL/Web_Files/docs/AAL-Getting%20Bodies%20into%20Contact%20-%20the%20Despair%20and%20Joy.pdf, last checked on 2019-05-22.
- [63] S. Vanrostenberghe, M. Clarin, Y. Shin, B. Droesbeke, V. V. der Mee, M. Doré, G. Marquis, J. Parantainen, T. Kannengieber, and Z. Barsoum. Improving the fatigue life of high strength steel welded structures by post weld treatments and specific filler materials (fatweldhss). Technical report, 9 Komponentensicherheit, 2015.
- [64] M. C. Vasco, P. Polydoropoulou, A. N. Chamos, and S. G. Pantelakis. Effect of corrosion and sandblasting on the high cycle fatigue behavior of reinforcing b500c steel bars. *Frattura ed Integrità Strutturale*, 11(42):9–22, 2017.

- [65] R. T. S. C. D. D. Vishnu Venugopal Poovakaud, Carlos Jiménez-Peña. Assessment of fretting fatigue in high strength steel bolted connections with simplified fe modelling techniques.-article under development. *Tribology International (ISSN 0301-679X)*, -.
- [66] R. Wagoner, J. Wang, and M. Li. Springback. *Metalworking: Sheet Forming(ASM Handbook)*, 14:733–755, 2006.
- [67] R. Willms. High strength steel for steel constructions. In *Nordic Steel Construction Conference-NSCC*, pages 597–604, 2009.
- [68] M. N. York). *Machinery’s Handbook*. Number v. 20. Industrial Press, 1977.
- [69] P. Zampieri, A. Curtarello, E. Maiorana, and C. Pellegrino. A review of the fatigue strength of shear bolted connections. *International Journal of Steel Structures*, pages 1–15, 2018.
- [70] Zwick/Roell. Dynamic and fatigue testing systems. URL: https://www.zwickroell.com/-/media/files/sharepoint/vertriebsdoku_br/99_765_dynamic_and_fatigue_testing_systems_en.pdf, last checked on 2019-06-24.
- [71] Zwick/Roell. Product information. servo-hydraulic load frames - ha series. URL: https://www.zwickroell.com/-/media/files/sharepoint/vertriebsdoku_pi/10_519_ha_series_pi_en.pdf, last checked on 2019-06-24.